



HAL
open science

Hydrology and small pelagic fish drive the spatio-temporal dynamics of springtime zooplankton assemblages over the Bay of Biscay continental shelf

Nina Grandremy, Jean-Baptiste Romagnan, Christine Dupuy, Mathieu Doray, Martin Huret, Pierre Petitgas

► To cite this version:

Nina Grandremy, Jean-Baptiste Romagnan, Christine Dupuy, Mathieu Doray, Martin Huret, et al.. Hydrology and small pelagic fish drive the spatio-temporal dynamics of springtime zooplankton assemblages over the Bay of Biscay continental shelf. *Progress in Oceanography*, 2023, 210, pp.102949. 10.1016/j.pocean.2022.102949 . hal-03921422

HAL Id: hal-03921422

<https://hal.science/hal-03921422>

Submitted on 3 Jan 2023

HAL is a multi-disciplinary open access archive for the deposit and dissemination of scientific research documents, whether they are published or not. The documents may come from teaching and research institutions in France or abroad, or from public or private research centers.

L'archive ouverte pluridisciplinaire **HAL**, est destinée au dépôt et à la diffusion de documents scientifiques de niveau recherche, publiés ou non, émanant des établissements d'enseignement et de recherche français ou étrangers, des laboratoires publics ou privés.

Progress in Oceanography

Hydrology and small pelagic fish drive the spatio-temporal dynamics of springtime zooplankton assemblages over the Bay of Biscay continental shelf.

--Manuscript Draft--

Manuscript Number:	PROOCE-D-22-00201R1
Article Type:	Full Length Article
Section/Category:	Biological Oceanography
Keywords:	Mesozooplankton; imaging analysis; time-consistent spatial patterns; ecosystem structure; spring habitat; Multi Factor Analysis; Bay of Biscay
Corresponding Author:	Nina Grandremy, Ph.D IFREMER Nantes, FRANCE
First Author:	Nina Grandremy, Ph.D
Order of Authors:	Nina Grandremy, Ph.D Jean-Baptiste Romagnan Christine Dupuy Mathieu Doray Martin Huret Pierre Petitgas
Abstract:	<p>As mesozooplankton is the preferential prey of small pelagic fish (SPF), environmentally-driven mesozooplankton dynamics can have critical effects on SPF population dynamics. Despite previous studies on SPF habitats' dynamics, hydrological landscapes and mesozooplankton dynamics in the Bay of Biscay (BoB), knowledge gaps persist at the BoB regional-scale pelagic ecology and in particular about the mesozooplankton assemblages and their long-term space-time patterns. Here, we present 16 years of spring mesozooplankton assemblage interannual spatial dynamics over the BoB continental shelf and we describe the correlations between the mesozooplankton space-time patterns and those in hydrology, primary producers and SPF. We gathered data originating from the PELGAS surveys (2004-2019) and remote sensing products. Mesozooplankton samples were collected with a 200-μm mesh size WP2 net vertically towed from 100 m depth (or 5 m above the sea floor) to the surface. They were analysed with imaging and deep-learning tools and the biomass in 24 coarse taxonomic groups was calculated. Automated procedures for spatial gridding and missing data imputation enable the generation of yearly maps time series with the same spatial resolution across the pelagic ecosystem components and years. These comprehensive multivariate datasets were analysed with a multi-table method known as Multiple Factor Analyses to depict time-consistent spatial patterns in each ecosystem component and the temporal variability around them. Finally, the main time-consistent spatial patterns in the hydrology, primary producers and SPF ecosystem components were used as predictors in generalized linear models, to explain those in the mesozooplankton. Mesoscale coastal-offshore and north-south gradients were the main patterns observed in each of the pelagic ecosystem components studied. The spatial patterns in the mesozooplankton assemblage were stable, without any significant changes detected in the taxonomic composition nor its spatial structure over the studied period. Small copepods, gelatinous and meroplanktonic organisms characterised coastal areas. Euchaetidae and meroplanktonic crustaceans' larvae displayed higher biomass in the northern part of the BoB while Metridinidae, Cladocera, Appendicularia and Echinodermata had higher biomass in the southern part. Surface and bottom water temperature, salinity-related parameters, water column stratification and SPF biomasses were the variables that best explained the observed space-time patterns in the mesozooplankton communities.</p>
DOI:	10.1016/j.pcean.2022.102949

1 Hydrology and small pelagic fish drive the spatio-temporal dynamics of
2 springtime zooplankton assemblages over the Bay of Biscay continental
3 shelf.

4 **AUTHORS AND AFFILIATIONS**

- 5 • Nina GRANDREMY ^a

6 ^a DECOD (Ecosystem Dynamics and Sustainability), IFREMER, INRAE, Institut Agro, Nantes,
7 Centre Atlantique - Rue de l'Île d'Yeu - BP 21105 - 44311 Nantes Cedex 03, France. E-mail
8 address: nina.grandremy@ifremer.fr

- 9 • Jean-Baptiste ROMAGNAN ^a

10 ^a DECOD (Ecosystem Dynamics and Sustainability), IFREMER, INRAE, Institut Agro, Nantes,
11 Centre Atlantique - Rue de l'Île d'Yeu - BP 21105 - 44311 Nantes Cedex 03, France. E-mail
12 address: jean.baptiste.romagnan@ifremer.fr

- 13 • Christine DUPUY ^b

14 ^b BIOFEEL, UMRI LIENSs, La Rochelle Université / CNRS. E-mail address: cdupuy@univ-lr.fr

- 15 • Mathieu DORAY ^a

16 ^a DECOD (Ecosystem Dynamics and Sustainability), IFREMER, INRAE, Institut Agro, Nantes,
17 Centre Atlantique - Rue de l'Île d'Yeu - BP 21105 - 44311 Nantes Cedex 03, France. E-mail
18 address: mathieu.doray@ifremer.fr

- 19 • Martin HURET ^c

20 ^c DECOD (Ecosystem Dynamics and Sustainability), IFREMER, INRAE, Institut Agro, Brest,
21 France. E-mail address: martin.huret@ifremer.fr

- 22 • Pierre PETITGAS ^d

23 ^d IFREMER, RBE, Centre Atlantique, 44311, Nantes Cedex 03, France. E-mail address:
24 pierre.petitgas@ifremer.fr

25 **CORRESPONDING AUTHORS**

26 Nina GRANDREMY: ninagrandremy@hotmail.fr

27 Jean-Baptiste ROMAGNAN: jean.baptiste.romagnan@ifremer.fr

28 **ABSTRACT**

29 As mesozooplankton is the preferential prey of small pelagic fish (SPF),
30 environmentally-driven mesozooplankton dynamics can have critical effects on SPF
31 population dynamics. Despite previous studies on SPF habitats' dynamics,
32 hydrological landscapes and mesozooplankton dynamics in the Bay of Biscay (BoB),
33 knowledge gaps persist at the BoB regional-scale pelagic ecology and in particular
34 about the mesozooplankton assemblages and their long-term space-time patterns.
35 Here, we present 16 years of spring mesozooplankton assemblage interannual spatial
36 dynamics over the BoB continental shelf and we describe the correlations between the
37 mesozooplankton space-time patterns and those in hydrology, primary producers and
38 SPF. We gathered data originating from the PELGAS surveys (2004-2019) and remote
39 sensing products. Mesozooplankton samples were collected with a 200- μ m mesh size
40 WP2 net vertically towed from 100 m depth (or 5 m above the sea floor) to the surface.
41 They were analysed with imaging and deep-learning tools and the biomass in 24
42 coarse taxonomic groups was calculated. Automated procedures for spatial gridding
43 and missing data imputation enable the generation of yearly maps time series with the
44 same spatial resolution across the pelagic ecosystem components and years. These
45 comprehensive multivariate datasets were analysed with a multi-table method known
46 as Multiple Factor Analyses to depict time-consistent spatial patterns in each
47 ecosystem component and the temporal variability around them. Finally, the main
48 time-consistent spatial patterns in the hydrology, primary producers and SPF
49 ecosystem components were used as predictors in generalized linear models, to
50 explain those in the mesozooplankton. Mesoscale coastal-offshore and north-south
51 gradients were the main patterns observed in each of the pelagic ecosystem
52 components studied. The spatial patterns in the mesozooplankton assemblage were
53 stable, without any significant changes detected in the taxonomic composition nor its
54 spatial structure over the studied period. Small copepods, gelatinous and
55 meroplanktonic organisms characterised coastal areas. Euchaetidae and
56 meroplanktonic crustaceans' larvae displayed higher biomass in the northern part of
57 the BoB while Metridinidae, Cladocera, Appendicularia and Echinodermata had higher
58 biomass in the southern part. Surface and bottom water temperature, salinity-related
59 parameters, water column stratification and SPF biomasses were the variables that

60 best explained the observed space-time patterns in the mesozooplankton
61 communities.

62

63 **KEYWORDS**

64 Mesozooplankton, imaging analysis, time-consistent spatial patterns, ecosystem
65 structure, spring habitat, Multi Factor Analysis, Bay of Biscay.

66

67 **HIHGLIGHTS**

- 68 • Taxonomically and spatially-resolved zooplankton dataset over 16 years in
69 spring
- 70 • Time-consistent zooplankton composition spatial structure with multi-table
71 analysis
- 72 • Explanation of zooplankton spatial patterns with gradients in the pelagic
73 ecosystem
- 74 • Zooplankton spatial pattern underpinned by taxonomic composition and size
75 structure
- 76 • River plumes, temperature gradients and pelagic fish correlated zooplankton
77 pattern

78 1 Introduction

79 Mesozooplankton is the preferential prey of small pelagic fish (SPF, e.g. sardine
80 and anchovy; Plounevez and Champalbert, 1999; Van Der Lingen, 2002; Bachiller and
81 Irigoien, 2015; Fonseca et al., 2022). It is therefore a key trophic link that enables the
82 transfer of matter and energy from the primary production to higher trophic levels in
83 oceanic (Banse, 1995), upwelling ecosystems (Rykaczewski and Checkley, 2008) as
84 well as in continental shelf ecosystems (Irigoien et al., 2008; Dessier et al., 2018;
85 Noyon et al., 2022).

86 The short generation time of mesozooplankton and their sometimes non-linear
87 response to environmental changes make them sensitive to environmental variability
88 from small spatio-temporal scales (*i.e.* Romagnan et al., 2015, 2016) to long term,
89 global scale climate change (Hays et al., 2005; Batchelder et al., 2012; González-Gil
90 et al., 2015). Yet, the diversity of taxa, morphologies and size ranges often make
91 difficult to sample, analyse and model this important ecosystem component at the
92 appropriate spatio-temporal as well as biological resolutions (Mitra and Davis, 2010).
93 Further, the diversity of mesozooplanktonic organisms' life cycles and habitat
94 requirements translate into a variety of community dynamics that may require local to
95 large scales, and populations to communities' studies for their understanding.

96 Numerous studies suggest a potentially critical effect of environmentally driven
97 mesozooplankton dynamics on SPF population dynamics in various ecosystems
98 worldwide (*i.e.* Cury et al., 2000; Van Der Lingen, 2002; Rykaczewski and Checkley,
99 2008; Capuzzo et al., 2018). In the European waters, recent studies highlighted the
100 probable bottom-up effects of mesozooplankton-mediated decline in SPF body
101 condition and size in the Gulf of Lion (NW Mediterranean, Saraux et al., 2019). The
102 authors hypothesized that a decadal shift towards smaller mesozooplanktonic species
103 in the Mediterranean adversely affected the potential energy income of SPF (Queiros
104 et al., 2019 but see Feuilloley et al., 2022). A similar decadal trend in the decline in
105 SPF size at age has recently been evidenced over the 2000-2015 period (Doray et al.,
106 2018b), throughout the French continental shelf of the Bay of Biscay (hereafter BoB),
107 an open ocean bay delimited by the Spanish coast (south) and the French coast (east
108 & north). However, a comprehensive explanatory study still needs to be set up. This
109 study is a first step towards this goal, and aims at understanding the mesozooplankton

110 habitat distribution, and its correlations with variables describing the pelagic ecosystem
111 components, from hydrology (water temperature, salinity, water column stratification
112 index) to higher trophic levels (SPF).

113 A corpus of data and studies on the SPF habitats' patterns and dynamics exists
114 in the BoB (Petitgas et al., 2018; Doray et al., 2018c, 2022), as well as for hydrological
115 landscapes (Koutsikopoulos et al., 1998; Castaing et al., 1999; Planque et al., 2004;
116 Guillaud et al., 2008). Distribution patterns of mesozooplankton have also been
117 described but in the south-eastern area of the BoB only (Albaina and Irigoien, 2007a;
118 Dessier et al., 2018) and in the adjacent Cantabrian shelf (Albaina and Irigoien, 2007b;
119 Iriarte et al., 2022). Coastal waters show larger biomass and smaller organisms than
120 offshore waters (Sourisseau and Carlotti, 2006; Vandromme et al., 2014), and are
121 dominated by copepods and meroplanktonic organisms (Irigoien et al., 2008; Dessier
122 et al., 2018). Mesoscale oceanographic structures *i.e.* river plumes and shelf-break
123 fronts (Albaina and Irigoien, 2004, 2007b), hydrological features (*i.e.* water column
124 stratification), winter mixing and microphytoplankton abundance were identified as
125 drivers of mesozooplankton dynamics (González-Gil et al., 2015; Dessier et al., 2018).
126 Nevertheless, important knowledge gaps persist at the scale of the BoB and small
127 pelagic fish populations, as the spatial coverage of existing mesozooplankton studies
128 was consistently focused on the south of the BoB (South of 46°30N) although the North
129 is ecologically important *e.g.* as SPF spawning, feeding and nursery habitats (Bellier
130 et al., 2007; ICES, 2010). In addition, currently available mesozooplankton space-time
131 data series are often short: the longest spatially resolved series spans from 2003 to
132 2013 (Dessier et al., 2018), making the detection of long term changes detected in
133 many other ecological components (Chust et al., 2022) more difficult for the
134 mesozooplankton. Therefore, important uncertainties remain about the patterns of
135 mesozooplankton assemblages and their long-term space-time evolution, at the scale
136 of the entire BoB, in the context of accelerating ecological changes due to the local
137 effects of global warming (Chust et al., 2022).

138 Here, we present the first comprehensive space-time analysis of the
139 mesozooplankton community over 16 years (2004 to 2019), in spring, over the BoB
140 continental shelf. The spatial coverage of our study spans from the coast to the shelf
141 break, and from the eastern Spanish coast to southern Brittany coastal waters,
142 therefore encompassing the whole French BoB continental shelf (Fig. 1).

143 Mesozooplankton samples collected during the pelagic ecosystem survey PELGAS
144 (Doray et al., 2018c) were analysed with imaging tools (Gorsky et al., 2010; Colas et
145 al., 2018) to achieve a coarse but consistent taxonomic resolution throughout the
146 series. The homogeneity and completeness in the data spatial resolution over time was
147 guaranteed using a gridding smoothing procedure (Masse et al., 2018 section 3) and
148 a missing data imputation technique (Josse and Husson, 2016) when necessary. The
149 same data preparation procedure was applied to concomitant hydrology, primary
150 producers and SPF data series originating from the PELGAS surveys and remote
151 sensing data to generate a comprehensive dataset with the same space-time
152 resolution across the pelagic ecosystem components. Our goal is to explore the
153 variability in the spatial patterns over time in the BoB mesozooplankton assemblage
154 and how they correlate with the other pelagic ecosystem components. The
155 mesozooplankton component was studied here considering its estimated biomass to
156 produce time series of maps that could be integrated in future zooplankton modelling
157 studies. This new data could be integrated to marine food web studies, which are often
158 based on biomass data. This spatial ecology approach is a first step in identifying
159 potential bottom-up and top-down controls exerted on the BoB mesozooplankton
160 assemblage, in a climate change context.

161 2 Materials and methods

162 2.1 The PELGAS survey

163 The PELGAS integrated survey takes place every year in spring since 2000, over
164 the French continental shelf of the BoB. The aim of this survey is to assess small
165 pelagic fish biomass and monitor the pelagic ecosystem, to inform ecosystem based
166 fisheries management. Concomitantly with fish data, hydrology, phyto- and zoo-
167 plankton samples and megafauna sightings (marine mammals and seabirds) are
168 collected to build long-term spatially-resolved time series of the BoB pelagic
169 ecosystem. The PELGAS sampling strategy combines en-route data collection (small
170 pelagic fish and megafauna) during the day, with fixed points, depth-integrated
171 hydrology and plankton sampling during the night (Fig. 1). Detailed PELGAS survey
172 protocols can be found in Doray et al., 2018b and 2021.

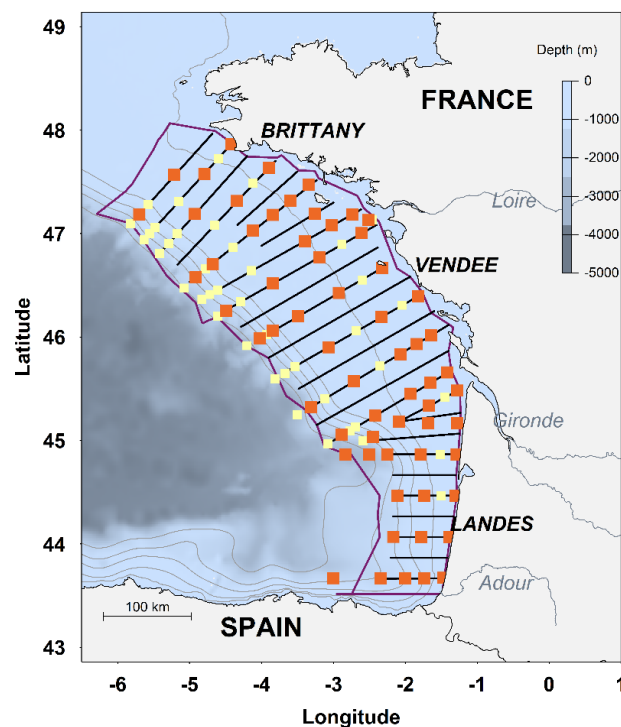


Fig. 1: PELGAS sampling scheme. Solid black lines: acoustic prospection transects for the evaluation of SPF biomass. Squares: Fixed-point water column sampling for hydrology parameters (light yellow) or hydrology parameters and plankton (orange) sampling. Note that the fixed-point geographical positions and sampling may change from year to year. Solid purple line: area considered for this study. Light grey lines: 100 to 500 m isobaths.

173 **2.2 Mesozooplankton samples collection**

174 Mesozooplankton samples were collected with vertical hauls of 200- μm mesh size
175 WP2 net, from 100 m depth (or 5 m above the sea floor) to the surface. In 2004 and
176 2005, the sampling maximum depth was 200 m. Since 2014, the net has been
177 equipped with a flowmeter (Hydrobios) to measure the sampled water volume. Before
178 2014, the sampled water volume was estimated by multiplying the deployed cable
179 length by the net opening surface (0.25 m²). From 2004 to 2019, the number of
180 sampling points varied between 41 and 64 per year, due to adjustments in the sampling
181 strategy and weather conditions. Between 2004 and 2016, 699 samples were collected
182 and preserved in 4% formaldehyde on board for further analysis back on land. Between
183 2017 and 2019, 190 samples were collected and were analysed live on board. Both
184 sets of samples were analysed with imaging instruments.

185 **2.3 Mesozooplankton analyses and data**

186 The preserved samples (2004-2016) were digitized on land with the ZooScan, a
187 waterproof flatbed scanner generating 16 bit gray-level high resolution images (pixel
188 size: 10.56 μm , 2400 dpi) (Gorsky et al., 2010). Prior to digitization, the samples were
189 size-fractionated with a 1 mm sieve, into organisms > 1 mm and <1 mm size fractions,
190 to avoid underestimation of large and rare objects due to subsequent subsampling.
191 Then, both fractions were separately subsampled with a Motoda splitter, to obtain sub-
192 samples containing 500-1500 objects. Each subsample was imaged after manual
193 separation of objects on the scanning tray, to minimize the occurrence of touching
194 objects (Vandromme et al., 2012). Remaining touching objects were manually digitally
195 separated with a custom Zooprocess tool to ensure the quality of further identifications
196 and counts. From 2017 onwards, the samples were analysed live on board with the
197 ZooCAM, an in-flow imaging instrument (pixel size: 10.3 μm) allowing the quasi real
198 time analysis of samples (Colas et al., 2018). Samples were split as a single fraction
199 with a Motoda splitter before being digitized. The agreement between the ZooScan
200 and the ZooCAM in identifying similar communities and producing similar total
201 mesozooplankton abundances and size distributions was demonstrated earlier (Colas
202 et al., 2018). All raw images generated with both instruments were processed to obtain
203 individual vignettes of each object digitized and associated morphological features,

204 including the size in pixels of each object. All individual planktonic vignettes were
205 classified using Ecotaxa (Picheral et al., 2017), a dedicated online tool that combines
206 a Random-Forest and a Convolutional Neural Network to achieve automatic
207 identification, which is now a classic semi-automatic identification procedure. Each
208 identified object, originating from both instruments, was then visually checked and
209 explicitly validated or corrected when necessary, using Ecotaxa again. Eventually,
210 2,135,401 objects were analysed and sorted into 24 broad taxonomic groups, to
211 achieve a trade-off between the diversity of the taxa seen in the area, and the
212 identification skills of experts who validated the automatic classification results. The
213 taxonomic resolution is detailed in Table 1. Some taxonomic groups aggregate a
214 diversity of species. For example, the group “Eumalacostraca” comprised adult forms
215 of crustaceans such as Amphipods, Decapods and Isopods. The group “Meroplankton
216 crustacean larvae” consisted of larval forms of meroplanktonic crustaceans, for
217 example Cirripedia, Brachyours and Decapods zoe. The category “Crustacean nauplii”
218 grouped the nauplii forms of holoplanktonic crustaceans, mostly copepods (Table 1).
219 Non-living objects (i.e. detrituses, large aggregates, artefacts) and remaining multiple
220 objects were excluded from the dataset.

221 Then, the biomass expressed in μg Dry Weight of each object was calculated from
222 each object’s individual surface in pixels converted to mm^2 , following Lehet and
223 Hernández-León (2009) and Garijo and Hernández-León (2015) (Table 1). These
224 equations are a common way to estimate biomasses of coarse zooplankton taxa and
225 were used in zooplankton studies in the Southern Ocean (Stirnemann et al., 2021;
226 Kerkar et al., 2022), tropical oceans and temperate environments (Marcolin et al.,
227 2015; Garcia-Herrera et al., 2022; Giering et al., 2019; Makhlof Belkahia et al., 2021;
228 Noyon et al., 2022) and at the global scale (Hernández-León et al., 2020; Siviadan et
229 al., 2022), in open ocean as well as in shelf seas. The biomass of each taxonomic
230 group was calculated at every sampling station, by summing the objects’ biomass
231 within each taxonomic group, multiplied by the subsampling ratio and divided by the
232 sampled water volume, to obtain the biomass expressed in μg Dry Weight. m^{-3} for each
233 taxa, at each sampling point. The organisms’ size considered in this study ranged
234 between 0.3 and 3.4 mm ESD (large mesozooplankton). Data from both instruments
235 were finally assembled to form a spatially-resolved dataset comprising 24
236 mesozooplankton taxa over 16 years from 2004 to 2019.

Table 1: Mesozooplankton taxonomic groups used to characterise mesozooplankton spring community in the Bay of Biscay; the conversion equations of body area “A” (mm²) into dry weight (µg Dry Weight) were found in Lehette & Hernandez – Leon (2009) and Garijo & Hernandez – Leon (2015).

Organisms	Taxonomic groups	Code	Dry weight
Copepods	Acartiidae	Acart	$43.97 * A^{1.52}$
	Calanidae	Cal	
	Centropagidae	Centrop	
	Euchaetidae	Euch	
	Metridinidae	Metri	
	Temoridae	Temo	
	Other Calanoida	Calano	
	Cyclopoida	Cyclo	
	Harpacticoida	Harpact	
	Poecilostomatoida	Poecil	
Other crustaceans	Eumalacostraca	Eumal	$43.97 * A^{1.52}$
	Meroplankton crustacean larvae	Larv_mero	
	Crustacean nauplii	Npl_crust	
	Cladocera	Clad	
General euphausiids	Shrimp-like	Shrimp	$49.58 * A^{1.48}$
Chaetognaths	Chaetognaths	Chaeto	$23.45 * A^{1.19}$
Cnidarian: Siphonophores	Siphonophores	Sipho	$43.17 * A^{1.02}$
Other gelatinous plankton	Appendicularians	Append	$4.03 * A^{1.24}$
	Thaliacea	Thal	
	Other Cnidarians	Cnid	
Other plankton	Bivalvia larvae	Biv	$43.38 * A^{1.54}$
	Fish larvae	Actin	
	Echinodermata larvae	Echin	
	Thecosomata	Thec	

238 **2.4 Hydrology and primary producers data**

239 At-station vertical profiles were performed with a conductivity-temperature-depth
240 (CTD, SeaBird SBE19 + V2) probe fitted with a fluorimeter and Niskin bottles, to
241 conduct hydrological and phytoplankton sampling. Several water column structure
242 descriptors were calculated from CTD casts, at each sampling station (Table 2): the
243 surface salinity (mean between 2 and 7 m), the bottom temperature (value recorded at
244 5 m above the seabed), the equivalent freshwater height, and three water column
245 stratification indices: the potential energy deficit, the mixed layer maximum depth, and
246 the pycnocline depth. The equivalent freshwater height is an index of river plume
247 influence, which measures the freshwater height over the water column, considering a
248 salinity reference value set at 35.5 psu. It better integrates the recent history and local
249 influence of river run-offs and is less sensitive to vertical mixing than surface salinity.
250 The deficit of potential energy is an index of water column stratification, defined as the
251 energy necessary to homogenise the water density over the water column. A detailed
252 description of these water column descriptors can be found in Huret et al. (2013).

253 Water samples collected with the Niskin bottles at the surface were filtered on board,
254 stored at -80°C and further analysed by spectrophotometry back on land, to estimate
255 the total and size-fractionated chlorophyll-a concentration (pico- (< 3 µm), nano- (3-20
256 µm) and micro-phytoplankton (> 20 µm)). The water column integrated chlorophyll-a
257 concentration was estimated using the fluorescence data from the vertical profiles
258 which was calibrated with the actual measures of chlorophyll-a concentrations at three
259 depths (surface, deep chlorophyll maximum, and below the thermocline).

260 Sea surface temperatures (SST) and surface chlorophyll-a concentrations from
261 remote sensing data were downloaded from <https://marine.copernicus.eu/> (named as
262 SST_ATL_SST_L4_REP_OBSERVATIONS_010_026 and
263 OCEANCOLOUR_ATL_CHL_L4_REP_OBSERVATIONS_009_098, respectively).
264 The downloaded SST data products were derived from AVHRR sensors of NOAA
265 satellites daily products, and interpolated to fill in missing data due to the clouds,
266 following Saulquin and Gohin (2010). Surface chlorophyll-a concentration data were
267 derived from several sensors (SeaWiFS, MERIS, MODIS) and processed following
268 Gohin (2011).

269 Table 2: Parameters used to describe the hydrological conditions and the primary producers
 270 structure in the Bay of Biscay, in spring.

Ecosystem component	Parameter		Code	Units	Time series	Source
Hydrology	Bottom temperature		BTemp	°C	2004 - 2019	PELGAS surveys
	Potential energy deficit		PotEDef	Kg.m ⁻¹ .m ⁻²		
	Equivalent freshwater height		EqFH	meters		
	Mixed layer depth		MLD			
	Pycnocline depth		PycnD			
	Surface salinity		SSal	psu		
	Surface temperature		STemp	°C		Satellite data
Primary producers	Size-fractionated surface chlorophyll-a concentration	< 3 µm	Chl3	mg.m ⁻³	2009 - 2019	PELGAS surveys
		3 - 20 µm	Chl-3-20			
		> 20 µm	Chl20			
	Total surface chlorophyll-a concentration		TotChl			
	Integrated chlorophyll-a		IntChl	mg.m ⁻²		
	Chlorophyll-a maximum concentration depth		ChIMD	meters		
	Chlorophyll-a concentration		satChl	mg.m ⁻²		Satellite data

271 2.5 Small pelagic fish biomass

272 Small pelagic fish acoustic densities were recorded at 10 knots during daytime,
 273 along transects using a calibrated monobeam echosounder operating at 38 kHz.
 274 Midwater trawl hauls were adaptively performed to identify to species the echotraces
 275 and provide their length, weight and age composition. Acoustic and biotic trawl data
 276 were combined using the standard methodology described in Doray et al. (2021) to
 277 derive biomass estimates per species and 5 cm length classes, within one nautical
 278 mile (1852 m) long Elementary Sampling Units along the survey track. Biomass
 279 estimates were expressed in tonnes per nautical miles square (tonnes.nm⁻²). The SPF
 280 species appearing in at least 50 % of the 16 PELGAS surveys considered (2004-2019)
 281 were selected to characterise the fish component. Selected species included boarfish
 282 (*Capros aper*), Atlantic chub mackerel (*Scomber colias*), Atlantic mackerel (*Scomber*

283 *scombrus*), Atlantic horse mackerel (*Trachurus trachurus*), Mediterranean horse
 284 mackerel (*Trachurus mediterraneus*), blue whiting (*Micromesistius poutassou*),
 285 European anchovy (*Engraulis encrasicolus*), European sardine (*Sardina pilchardus*)
 286 and sprat (*Sprattus sprattus*) (Table 3).

Table 3: Time series of small pelagic fish species considered by 5 cm length classes.

SPF species	Code	Length class	Time series (n years)
Boarfish (<i>Capros aper</i>)	CAPR-APE	(10, 15]	2004 - 2019 (9)
European anchovy (<i>Engraulis encrasicolus</i>)	ENGR-ENC	(5, 10]	2006 - 2019 (8)
		(10, 15]	2004 - 2019 (16)
		(15, 20]	
Blue whiting (<i>Micromesistius poutassou</i>)	MICR-POU	(15, 20]	2004 - 2017 (11)
		(20, 25]	2004 - 2019 (15)
		(25, 30]	2005 - 2019 (14)
European sardine (<i>Sardina pilchardus</i>)	SARD_PIL	(10, 15]	2005 - 2019 (13)
		(15, 20]	2004 - 2019 (16)
		(20, 25]	
Atlantic chub mackerel (<i>Scomber colias</i>)	SCOM-COL	(15, 20]	2004 - 2018 (14)
		(20, 25]	2004 - 2019 (16)
		(25, 30]	2004 - 2019 (15)
		(30, 35]	2004 - 2019 (14)
		(35, 40]	2005 - 2019 (9)
Atlantic mackerel (<i>Scomber scombrus</i>)	SCOM-SCO	(15, 20]	2005 - 2019 (11)
		(20, 25]	2004 - 2019 (16)
		(25, 30]	
		(30, 35]	
		(35, 40]	
European sprat (<i>Sprattus sprattus</i>)	SPRA-SPR	(5, 10]	2004 - 2019 (13)
		(10, 15]	2004 - 2019 (16)
Atlantic horse mackerel (<i>Trachurus trachurus</i>)	TRAC-TRU	(10, 15]	2004 - 2019 (16)
		(15, 20]	
		(20, 25]	
		(25, 30]	
Mediterranean horse mackerel (<i>Trachurus mediterraneus</i>)	TRAC_MED	(30, 35]	2004 - 2019 (13)
		(15, 20]	2005 - 2018 (10)
		(20, 25]	2006 - 2019 (10)
		(40, 45]	2006 - 2019 (9)

287 A summary of the data used in this study can be found in Fig. 2 (top panel).

288

2.6 Data gridding and missing data imputation

289 Although the biological and physico-chemical sampling are rather regular and
290 homogeneous on the PELGAS cruise (Doray et al., 2018c), the spatial resolution and
291 number of samples may vary across years and between variables. Therefore, a block
292 averaging procedure (Petitgas et al., 2009, 2014) was consistently applied on each of
293 the datasets before conducting any further analysis. All variable used were gridded
294 over a common spatial grid. The grid mesh size was set at 0.3° in both latitude and
295 longitude, a compromise between the grid mesh size commonly set at 0.25° in previous
296 studies based on spatially resolved datasets (Doray et al., 2018a; Masse et al., 2018;
297 Petitgas et al., 2018) and the distance between the mesozooplankton sampling
298 stations, to limit the number of grid cells without data. The grid origin x_0 was initially
299 positioned at 43°N and 6°W and then drawn randomly within a two cells radius, 300
300 times. Data were averaged in each grid cell for every origin position, in order to
301 minimize the influence of the origin position on gridded values. Finally, 300 mean
302 values were averaged to calculate a spatially smoothed estimate in each grid cell (Fig.
303 2, step 1). Grid cells having their center point inside the polygon defining the survey
304 area were kept for the analysis ($n = 121$) (Fig. 1). The block averaging step was
305 realized with the *EchoR R* library (Doray et al., 2013).

306 After the block averaging step, some cells were still empty (missing data). These
307 missing data are the consequence of missing sampling stations, especially in the
308 northern part of the BoB, mostly at the beginning of the time series (Appendix A, Table
309 A.1). To fill data gaps in particular grid cells and years, we applied a missing data
310 imputation procedure (Josse and Husson, 2016). Each variable was organized into
311 matrix form, grid cells x years. An algorithm based on iterative Principal Component
312 Analysis (PCA) was applied to each data matrix, to impute predicted data point values
313 to the empty cells (Fig. 2, step 2). The iterations were run until the difference between
314 two successive estimated values was smaller than a threshold (set at $1e-06$).
315 Sometimes, the final predicted values were negative. In this case, we imputed the
316 mean of the adjacent grid cells to the empty cell. A comparison of annual spatial
317 patterns and annual means, calculated with and without the imputed values, was used
318 as a quality check of the imputed values. This missing data imputation method was
319 implemented using the *MissMDA R* library (Josse and Husson, 2016).

320 Eventually, the complete dataset is composed of sets of gridmaps for parameters in
321 the hydrology, primary producers, mesozooplankton and SPF components. All the
322 gridmaps have the same spatial extent and resolution and span from 2004 to 2019,
323 except for primary producers dataset which span from 2009 to 2019.

324 **2.7 Data analysis**

325 All the data analyses were performed using the *R* statistical language version 4.0.3
326 (R Core Team, 2020). The analytic pipeline is organized as follow. First, we applied a
327 Multiple Factor Analysis (MFA, see below for details) on each ecosystem component
328 (Fig. 2, step 3). Then the mesozooplankton MFA results were used to input a
329 hierarchical clustering (Fig. 2, step 4). Finally, results from the hydrology, primary
330 producers and fish MFA were used as explanatory variables in Generalized Linear
331 Models (GLMs) to explain the observed mesozooplankton space-time patterns (Fig. 2,
332 step 5).

333 *2.7.1 Multiple Factor Analysis*

334 Multiple Factor Analysis (MFA, Escofier and Pagès, 1994; Pagès, 2014) has
335 recently been applied to characterise space-time patterns in series of multivariate
336 gridmaps of ecological variables (Abdi et al., 2013; Doray et al., 2018a; Petitgas et al.,
337 2018). MFA is a multi-table statistical method based on PCA and designed to analyse
338 3D structured datasets, in which the variables are organized in tables of the same size,
339 over time. Here, the grid cells correspond to the tables' rows (1st dimension: n
340 individuals), the variables the columns (2nd dimension: m variables), and the tables are
341 stacked (3rd dimension: p groups), to obtain a multivariate time series of yearly tables.
342 It is worth noticing that MFA applies even when the number of available variables differ
343 over time.

344 Similarly as with PCA and a 2D dataset, MFA results in summarizing a 3D dataset
345 into a factorial space, in which all individuals (*i.e.* grid cells), variables and tables
346 (years) can be represented (Pagès, 2014). Eventually, each grid cell can be located in
347 each year in the factorial space around its (time) average position and similarly for
348 each variable. MFA enables the estimation of a common multivariate correlation
349 structure over all years, and its associated time variability. The individuals being grid
350 cells here, the target structure is a spatial pattern with its time variability. For a detailed

351 description of MFA implementation, see Petitgas et al., 2018, § 3.3 - 3.5, pp 191-193,
352 and Doray et al., 2018 § 2.5-2.7, p 91.

353 *2.7.2 MFA implementation and principal components selection*

354 Specific MFAs were applied separately on the hydrology, primary producers,
355 mesozooplankton and SPF datasets, to characterize their space-time patterns. Data
356 from biotic components (primary producers, mesozooplankton and SPF) were
357 log-transformed to reduce the skewness in their distributions. Hydrology and primary
358 producers variables were centred and normalized in each year to account for the
359 differences in units and ranges. Mesozooplankton and SPF variables were centred
360 only (all variables in these two datasets have the same units), thus leaving the
361 differences in variance between years affect time variability. The MFAs were
362 implemented using the function *MFA* from the FactoMineR *R* library (Lê et al., 2008).

363 Similarly to a classic PCA, MFA can be used to reduce the dimensionality, filter
364 and synthesize complex datasets by selecting only a few first principal components
365 (*PCs*) for subsequent analyses. When using MFA on time resolved datasets, it is
366 important to consider not only the percentage of total variance explained by the MFA
367 *PCs* (Fig. 4), but also the number of significant correlations between each *PC* and the
368 years (*i.e.* tables) to assess the representativity of each *PC* over time (Pagès, 2014).
369 We selected the *PCs* that showed correlations with the years higher than a threshold
370 for at least half of the total number of years. Such threshold was estimated following
371 Pagès (2014), using the maximum value of correlation between years and high orders
372 *PCs*, here *PC.4* and *PC.5* (see the results of this procedure in Fig. 5).

373 Then, each selected *PC* was interpreted considering its correlation with the
374 variables. The variables retained to interpret the *PCs* showed a correlation coefficient
375 greater than |0.5| with the *PCs* for at least half of the total number of years. Further,
376 mean individuals' (grid cells') coordinates on the *PCs* were mapped at their
377 geographical positions. The MFA selected *PCs* were used as synthetic descriptors for
378 each of the ecosystem component datasets.

379 *2.7.3 Mesozooplankton space-time patterns: hierarchical clustering*

380 The average spatial structure of the mesozooplankton community was identified
381 by applying a Hierarchical Agglomerative Clustering (function *hclust* in *R* language,

382 Ward's method, Euclidean distance, without spatial constrain) on the mean individuals'
383 (grid cells') coordinates in the mesozooplankton MFA factorial space. The function
384 NbClust from the R library NbClust (Charrad et al., 2014) was used to determine the
385 optimal number of clusters through the calculation of thirty partitioning indices. The
386 best number of clusters is defined as the one suggested by the highest number of
387 indices. Then, grid cell clusters were mapped, to characterise regions with
388 time-consistent specific mesozooplankton assemblages. The taxonomic composition
389 of each cluster was assessed by calculating the annual mean of the variables (taxa) in
390 each cluster. Only the taxa showing a correlation coefficient greater than $|0.5|$ with the
391 mesozooplankton MFA *PCs* for at least half of the total number of years were
392 considered. Variables being centered, the annual mean biomass of a taxa within a
393 cluster represents its residual variation relative to the global mean taxon biomass over
394 all the grid cells and years. Finally, each grid cell in each year was associated to the
395 nearest cluster centroid in the MFA space to estimate the annual spatial distribution of
396 the clusters and to characterize the interannual variability in the clusters. The frequency
397 of grid cells affiliation within each cluster was also calculated over the time series, and
398 mapped.

399 *2.7.4 Correlates of the observed mesozooplankton space-time patterns*

400 The MFA *PCs* for the hydrology, primary producers and SPF ecosystem
401 components (referred to as predictors hereafter) were used as explanatory variables
402 in GLMs, where the MFA *PCs* for the mesozooplankton were the dependent variables.
403 For each *PC* selected in the mesozooplankton MFA, we first built a model using all the
404 predictors. We checked for collinearity in the predictors by using the Variance Inflation
405 Factor (VIF, Fox and Monette, 1992). A VIF value higher than five was used to identify
406 problematic multicollinearity among predictors. VIF was calculated using the *car* R
407 library (Fox and Weisberg, 2019). Predictors explaining less variance and displaying
408 high multicollinearity (VIF criterion) were removed. Then, a stepwise backward model
409 selection procedure was applied (function *stepAIC* in R language) to select the most
410 significant predictors based on Akaike's Information Criterion (AIC) (Burnham et al.,
411 2002). Models were considered significantly different when their AIC difference was
412 higher than two. Finally, an ANOVA was used on the model selected to rank the
413 predictors by their explicative power.

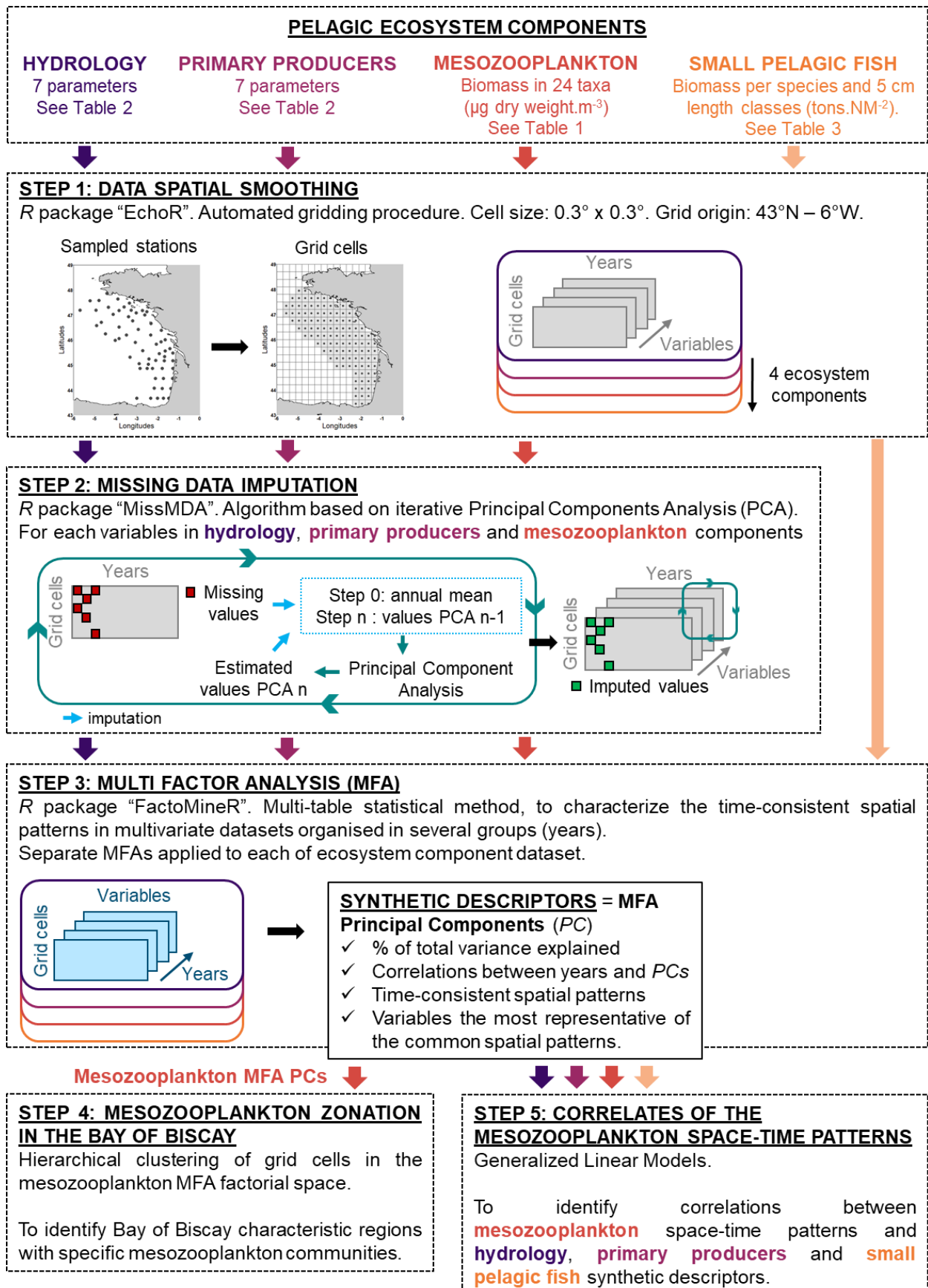


Fig. 2: Summary of the steps followed for the datasets construction and analysis.

415 **3 Results**

416 **3.1 Taxonomic composition and total biomass of the**
417 **mesozooplankton community**

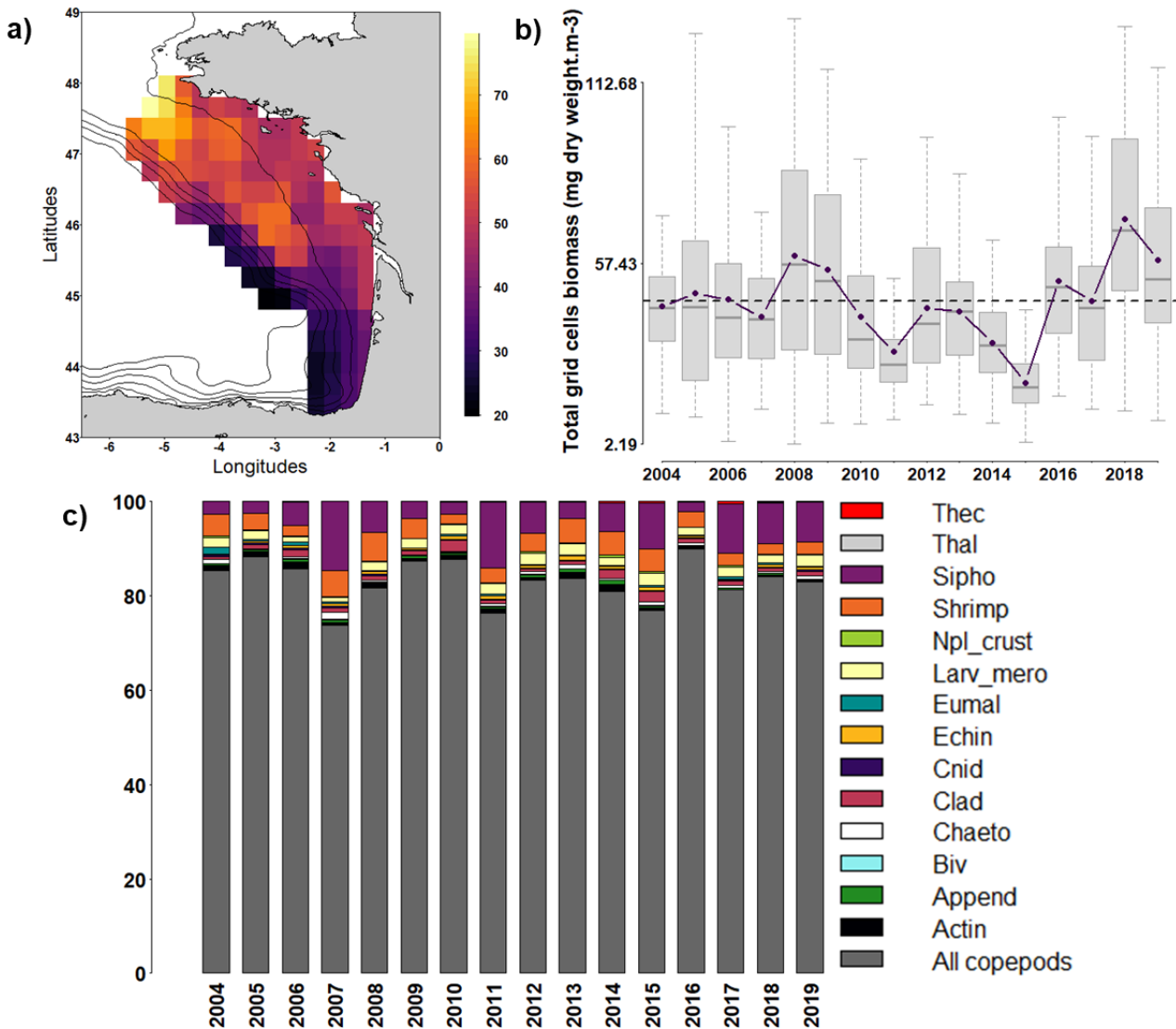


Fig. 3: (a) Mesozooplankton community total biomass (mg dry weight.m⁻³) mean map, averaged between 2004 and 2019. (b) Grid cells total biomass yearly distributions from 2004 to 2019. Boxplots: total biomass by grid cells (n = 121). The dashed line is the mean total biomass over the time series. Solid line: annual means. (c) Taxonomic groups relative contributions to the mesozooplankton community total biomass (percentage). The ten copepod groups were summed and plotted as one group for more clarity.

419 The mean map of total biomass per grid cell, from 2004 to 2019, revealed a
420 North-South gradient. Highest total biomass was observed north to 45.5°N between
421 the 100 m and 200 m isobaths, where the biomass ranged between 60 and 80 mg dry
422 weight.m⁻³, whereas the lowest values ranged between 20 and 30 mg dry weight.m⁻³
423 south of 45.5°N, on the continental shelf slope (Fig. 3a). Total biomass yearly
424 distributions did not show a clear temporal trend, but the lowest values occurred from
425 2010 to 2015. The lowest annual means occurred in 2011 and 2015 (30.5 ± 16 mg dry
426 weight.m⁻³ and 21 ± 8.6 mg dry weight.m⁻³, respectively), while the highest ones
427 occurred in 2008 and 2018 (59.8 ± 33.3 mg dry weight.m⁻³ and 71 ± 30.5 mg dry
428 weight.m⁻³, respectively) (Fig. 3b). The copepods dominated the mesozooplankton
429 community every year, contributing from 73% (2007) to 90% (2016) to the community
430 total biomass. Siphonophores was the second most important taxonomic group,
431 representing up to 14% of the total biomass in 2007 and 2011. These two groups had
432 opposite trends in their contributions, the years of minimum contribution of one
433 corresponding to the years of the maximum contribution of the other (Fig. 3c).

434 **3.2 MFA PCs selection for each ecosystem component.**

435 The first three *PCs* of the hydrology MFA (referred to as hydroMFA1, hydroMFA2
436 and hydroMFA3 hereafter) explained 72.8 % of the space-time variance in the
437 hydrology dataset (Fig. 4). In this case, the correlation threshold for retaining MFA *PCs*
438 as meaningful was set to 0.73 (see Methods section 2.7.2). All the years of the
439 hydrology time series showed correlations higher than 0.73 to the hydroMFA1 (n = 16)
440 and the hydroMFA2, except 2007 (hydroMFA2, n = 15). Ten years were correlated with
441 a coefficient > 0.73 to hydroMFA3 (Fig. 5a). The first *PC* of the primary producers MFA
442 (referred to as phytoMFA1 hereafter) explained 36.7 % of the space-time total variance
443 in the primary producers dataset (Fig. 4). It was the only *PC* showing correlation
444 coefficients with years (n = 11) higher than the threshold (here set to 0.67, see Methods
445 section 2.7.2) (Fig. 5b). The first two *PCs* of the mesozooplankton MFA (referred to as
446 zooMFA1 and zooMFA2 hereafter) explained 50.5 % of the space-time variance in the
447 mesozooplankton dataset (Fig. 4). All the years (n = 16) of the mesozooplankton time
448 series were correlated to the zooMFA1 with a coefficient higher than the threshold
449 (here set to 0.83, see Methods section 2.7.2). Ten years were correlated with a
450 coefficient > 0.83 to zooMFA2 (Fig. 5c). Finally, the first two *PCs* of the SPF MFA

451 (referred to as spfMFA1 and spfMFA2 hereafter) explained 45.5 % of the space-time
452 variance in the SPF biomass dataset (Fig. 4). Eleven years were correlated with a
453 coefficient higher than the threshold (here set to 0.9, see Methods section 2.7.2) to the
454 spfMFA1, and half the years ($n = 8$) were correlated to the spfMFA2 (Fig. 5d).
455 Eventually, eight MFA PCs were retained as synthetic descriptors for the next steps of
456 the analysis (*i.e.* hydroMFA1, hydroMFA2, hydroMFA3; phytoMFA1; zooMFA1,
457 zooMFA2; spfMFA1, spfMFA2).

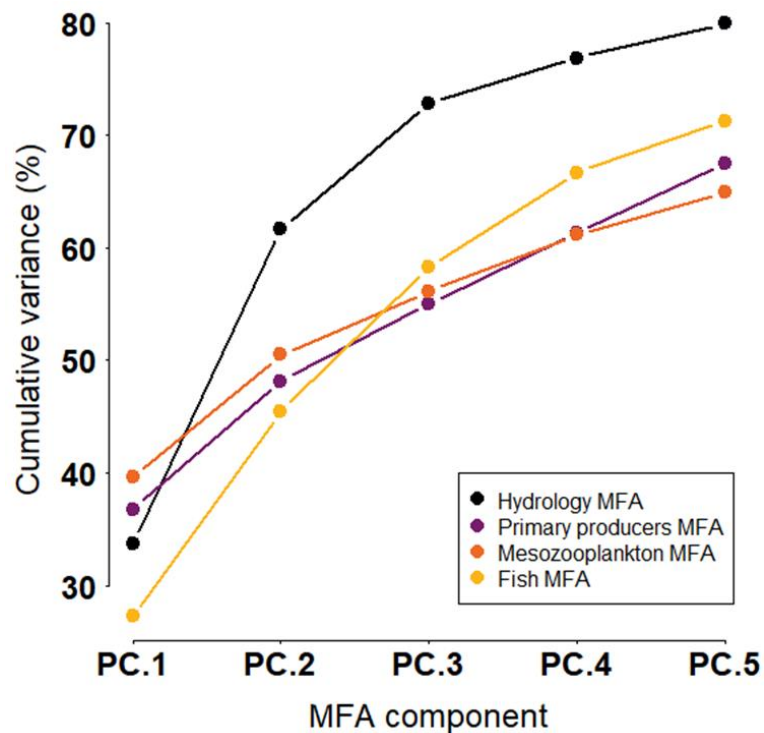


Fig. 4: Cumulative percentage of variance explained by the first five principal components of the Multiple Factor Analyses applied to the series of multivariate maps characterising hydrology, mesozooplankton and small pelagic fish (2004 - 2019) and primary producers data (2009 - 2019).

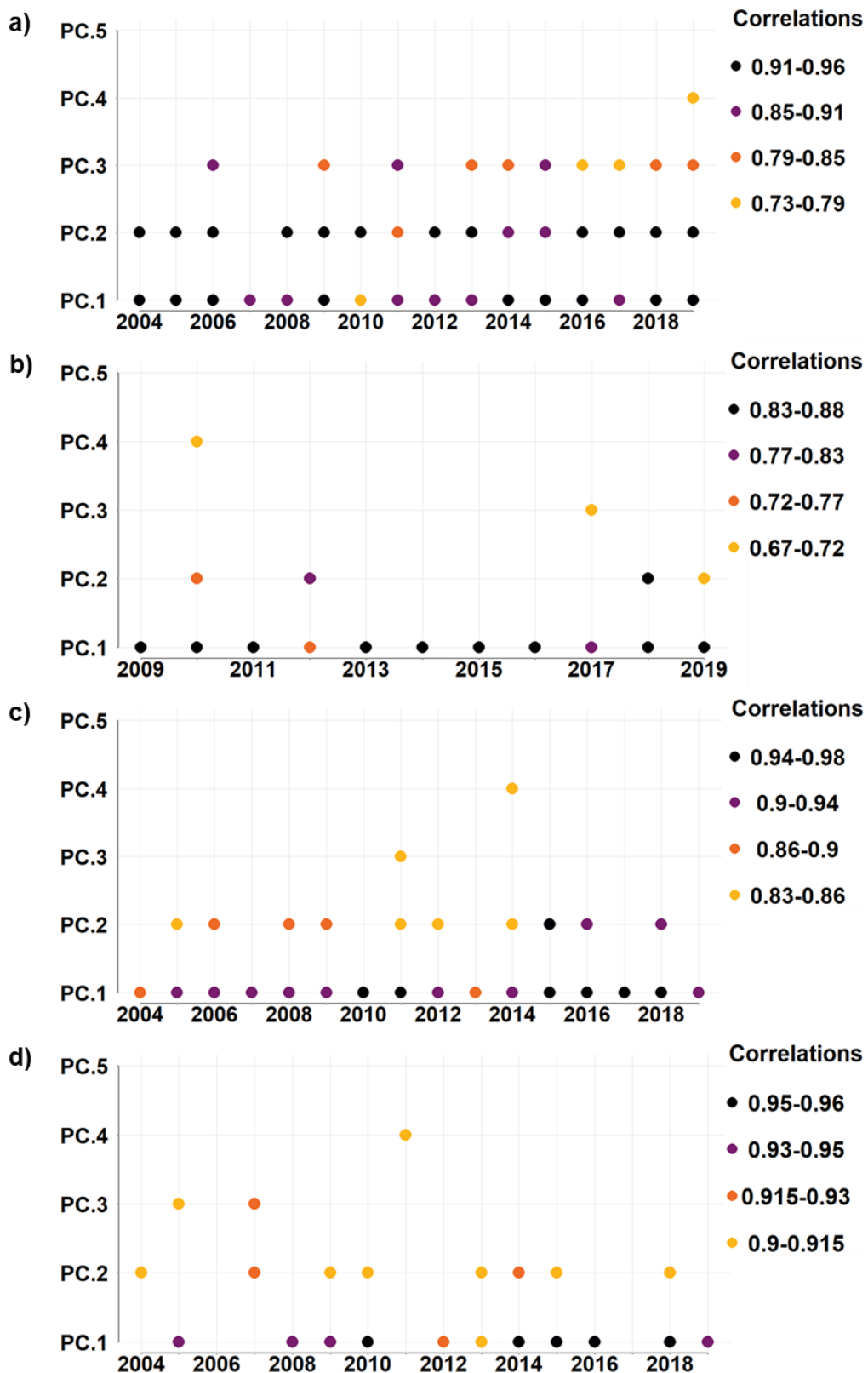


Fig. 5: Correlations between the years and the first five principal components of the Multiple Factor Analyses applied to the series of multivariate maps characterising (a) hydrology (2004 – 2019), (b) primary producers (2009 - 2019), (c) mesozooplankton (2004 – 2019) and (d) small pelagic fish (2004 - 2019). Only the correlations higher than the thresholds are shown (see Methods section 2.7.2).

459 **3.3 Mesozooplankton ecosystem component**

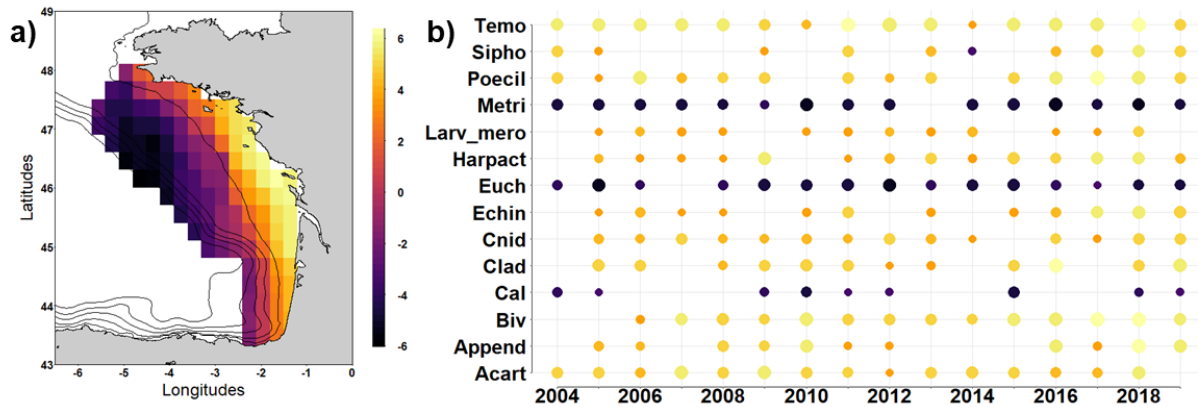
460 *3.3.1 Mesozooplankton MFA selected PCs*

461 Here we present the spatial patterns (MFA *PCs*) in the mesozooplankton
462 ecosystem component, based on the mapping of the mean individuals' (grid cells')
463 coordinates in the mesozooplankton MFA factorial space (Fig. 6a and c). The variables
464 defining the MFA *PCs* are shown in Fig. 6b and d.

465 The zooMFA1 showed a dominant coastal – offshore gradient in the
466 mesozooplankton community. This structure was highlighted by the highest values in
467 coastal areas, between the Loire estuary and the Arcachon Bay (Fig. 6a, lightest cells),
468 and the lowest along the shelf break, north to 46°N (Fig. 6a, darkest cells). Small
469 copepods, such as Acartiidae, Temoridae, Poecilostomatoida and Harpacticoida, as
470 well as Cnidarians, Cladocerans, Bivalvia, Echinoderms and meroplanktonic
471 crustaceans larvae groups displayed consistent positive correlations with zooMFA1
472 over the time series, revealing higher biomass in coastal areas. Significant positive
473 correlations with zooMFA1, and consequently higher biomass in coastal areas, were
474 also observed for appendicularians between 2005 and 2012 and between 2016 and
475 2019, indicating a higher variability across years for this taxon. On the contrary,
476 Metridinidae, Euchaetidae, and to a lesser extent Calanidae showed consistent
477 negative correlations with zooMFA1, and consequently high biomass offshore,
478 especially north to 46°N (Fig. 6b).

479 The zooMFA2 revealed a North – South gradient, highlighted by the highest
480 values in the northern part of the BoB along the Brittany southern coast (Fig. 6c, lightest
481 cells), and the lowest ones in the south, especially over the shelf break, south to 45.5°N
482 (Fig. 6c, darkest cells). The only taxa displaying a consistent positive correlation with
483 this component were the meroplanktonic crustaceans larvae, after 2008 (Fig. 6d),
484 showing higher biomass in the northern part of the BoB.

Principal component 1, mesozooplankton MFA



Principal component 2, mesozooplankton MFA

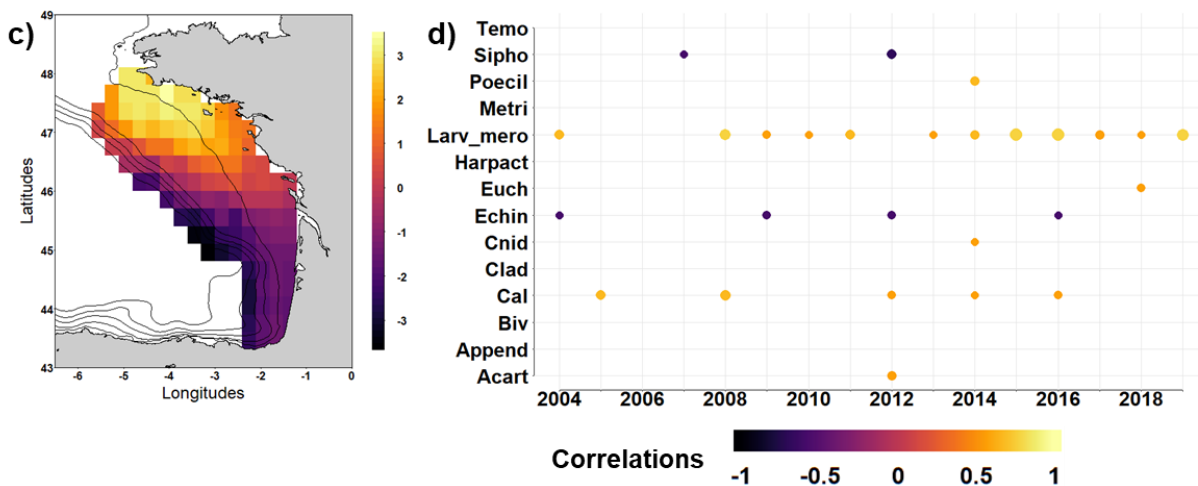


Fig. 6: Maps of mean individuals' (grid cells') coordinates on mesozooplankton Multiple Factor Analysis (MFA) principal component *PC.1* (a) and *PC.2* (c), and time series of significant correlations (> |0.5|) between the 24 taxonomic groups and MFA *PC.1* (b) and *PC.2* (d). The disk radii are proportional to the absolute value of the correlation coefficient. The mesozooplankton MFA was performed on the maps time series of 24 taxonomic groups biomass calculated from the PELGAS data, from 2004 to 2019 (Table 1).

485 3.3.2 Mesozooplankton zonation in the Bay of Biscay and its temporal evolution

486 The hierarchical clustering of the mean individuals' (grid cells') coordinates in the
 487 MFA factorial space made by the two selected *PCs* (*i.e.* zooMFA1 and zooMFA2,
 488 explaining 50.5 % of the mesozooplankton dataset total variance, Fig. 4), resulted in
 489 identifying three clusters, on the basis of the classification tree presented in Fig. 7a
 490 and the Nbclust method to identify significant clusters (Fig. 7b). The clusters' spatial
 491 distribution and their variability in time are presented in Fig. 8.

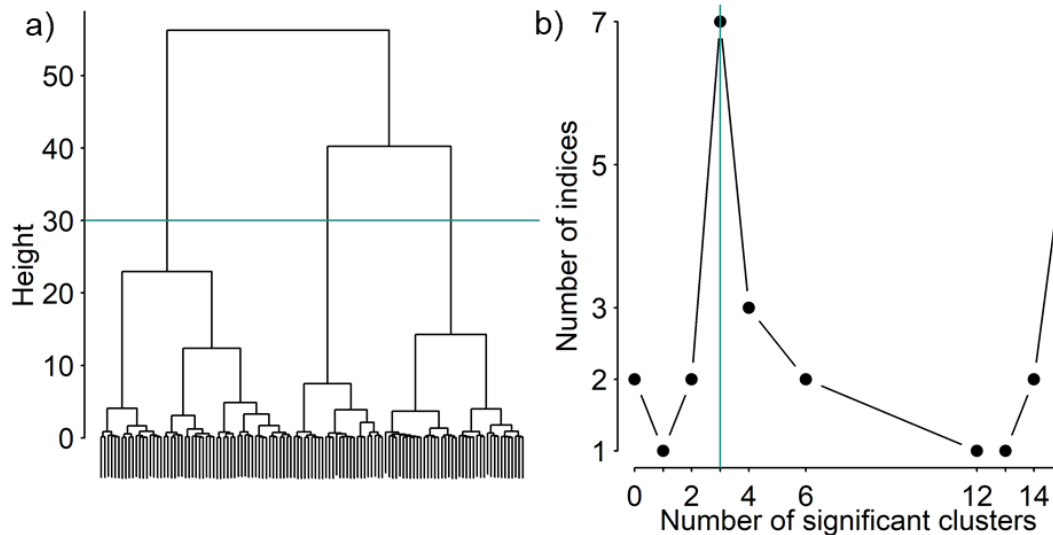


Fig. 7: (a) Classification tree of the hierarchical clustering of mean individuals (grid cells) coordinates in the mesozooplankton Multi Factor Analysis factorial space, made by the two selected mesozooplankton new descriptors (*i.e.* zooMFA1 and zooMFA2). (b) Number of clusters suggested by the Nbclust method (see section 2.7.3). Three clusters were retained (cut line in blue).

492

493 The time-consistent mesozooplankton spatial pattern combined coastal –
 494 offshore and north – south gradients (Fig. 8a). A coastal cluster (G2, blue / medium
 495 coloured cluster) extended from the Loire estuary to the south coast of the BoB, where
 496 all taxa displayed higher-than-average biomass except large copepods (*i.e.* Calanidae,
 497 Metridinidae and Euchaetidae) (Fig. 8c). A northern cluster (G3, yellow / light coloured
 498 cluster) was located North of 45.5°N, from offshore waters along the shelf break to the
 499 south Brittany coast. It was characterised mostly by Euchaetidae, and to a lesser extent
 500 Metridinidae, Calanidae and meroplanktonic crustaceans' larvae, all of them showing
 501 higher-than-average biomasses in this area (Fig. 8b). Finally, a southern cluster (G1,
 502 purple / dark coloured cluster) extended from the central – shelf areas, south of 46°N,
 503 mostly along the shelf break. Metridinidae dominated this southern mesozooplankton
 504 community, and Appendicularians, Cladocerans, Echinodermata, Euchaetidae and
 505 Siphonophorae also exhibited higher-than-average biomasses. On the contrary,
 506 Cnidarians, meroplanktonic crustaceans' larvae and Temoridae displayed the lowest
 507 overall biomass in this cluster (Fig. 8d). The spatial clusters corresponded to habitats
 508 of particular communities that were consistent in time. The largest temporal variability
 509 was located offshore in the northern cluster. The coastal and northern clusters covered

510 large spatial areas, whereas the southern cluster was less spatially extended and
511 confined to the small southern outer-shelf and shelf break (Fig. 8a).

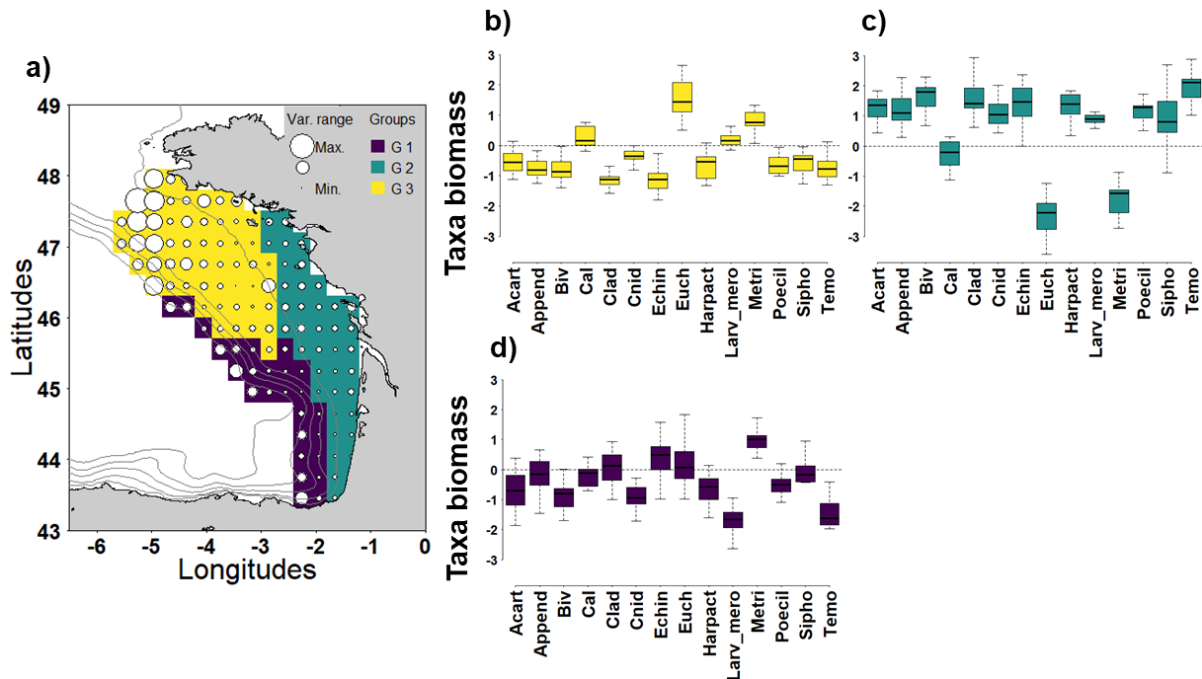


Fig. 8: (a) Time-consistent spatial patterns of the mesozooplankton community, derived from the hierarchical clustering of grid cells in the mesozooplankton Multiple Factor Analysis (MFA) space (two first principal components). White dots diameters are proportional to the inter-annual variability over the 16 years of the study. (b – d) Boxplots showing the inter-annual variability of the taxa biomasses ($\mu\text{g dry weight}\cdot\text{m}^{-3}$) in each cluster. The taxa shown are significantly correlated to the mesozooplankton MFA *PCs* with a frequency in time higher than 0.5. The horizontal dashlines mark the overall mean biomass (see Methods section 2.7.3).

512

513 Most of the grid cells within the coastal cluster G2 showed high occurrence
514 frequencies in time (> 0.8), meaning that they consistently belonged to this cluster over
515 time (Fig. 9c). The occurrence frequency of the grid cells within the southern and
516 northern offshore clusters were smaller and more variable over years. Some grid cells
517 along the shelf break between 46°N and 47°N switched between both clusters,
518 depending on the year (Fig. 9a and b). The annual distributions of clusters can be
519 found in the Appendix B, Fig. B1.

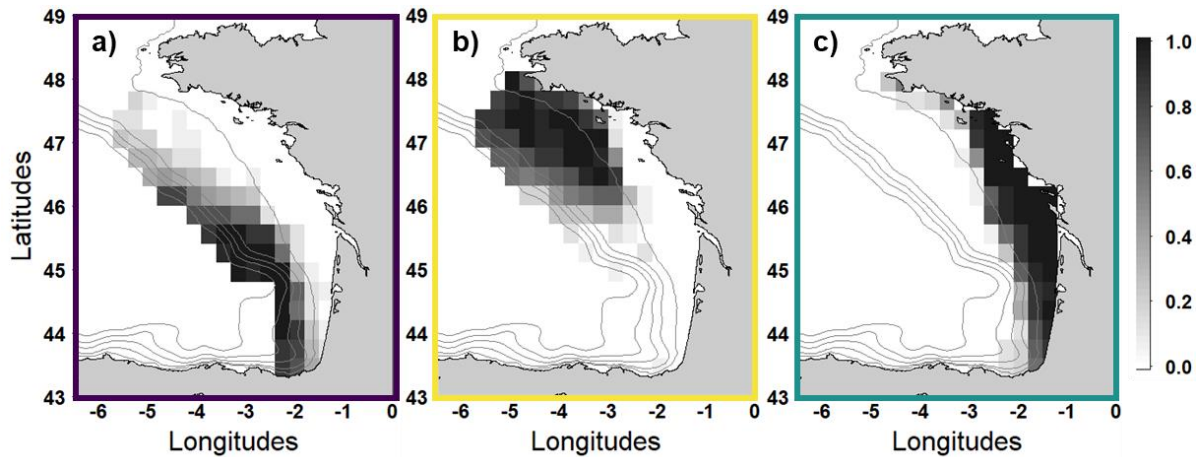


Fig. 9: Frequencies in time of grid cells' occurrences in each of the clusters forming the time-consistent spatial pattern: southern cluster G1 (a), northern cluster G3 (b), coastal cluster G2 (c).

521 **3.4 Other ecosystem components MFA selected *PCs***

522 *3.4.1 Hydrology ecosystem component*

523 Here we present the spatial patterns (MFA *PCs*) in the hydrology ecosystem
 524 component, based on the mapping of the mean individuals' (grid cells') coordinates in
 525 the hydrology MFA factorial space (Fig. 10a, c, e). The variables best correlated to the
 526 MFA *PCs* are shown in Fig. 10b, d, f.

527 The hydroMFA1 underpinned a dominant coastal – offshore gradient. This structure
 528 was highlighted by the lowest values off the Loire, Gironde and Adour estuaries (Fig.
 529 10a, darkest cells) and the highest along the shelf break in the northern part of the BoB
 530 (Fig. 10a, lightest cells). The surface salinity and the mixed layer maximum depth had
 531 consistently positive correlations with hydroMFA1, meaning that these variables drove
 532 the coastal-offshore gradient of hydroMFA1 with the highest values located offshore in
 533 the northern part of the BoB between 2004 and 2019. On the contrary, the equivalent
 534 freshwater height was constantly negatively correlated with hydroMFA1, revealing the
 535 influence of the river plumes in coastal waters. Finally, surface temperature displayed
 536 negative correlations with hydroMFA1 at the beginning (from 2004 to 2008) and at the
 537 end (from 2014 to 2019) of the time series, suggesting that it contributed significantly
 538 to the coastal – offshore gradient those years, with higher values in coastal areas (Fig.
 539 10b).

540 The hydroMFA2 displayed a north – south gradient, with the highest values in the
541 southern part of the BoB (Fig. 10c, lightest cells) and the lowest values in the northern
542 part of the BoB, along the Brittany southern coast, north to the Loire estuary (Fig. 10c,
543 darkest cells). The constant positive correlations of both surface and bottom
544 temperature with the hydroMFA2 throughout the series highlighted higher water
545 temperatures, in the south of the BoB, and colder water temperatures in the north (Fig.
546 10d).

547 The potential energy deficit was the only variable significantly correlated to the
548 hydroMFA3, with positive values (Fig. 10f), explaining the spatial pattern in hydroMFA3
549 with highest values in the middle of the shelf centered on the 100 m isobaths (Fig. 10e,
550 lightest cells).

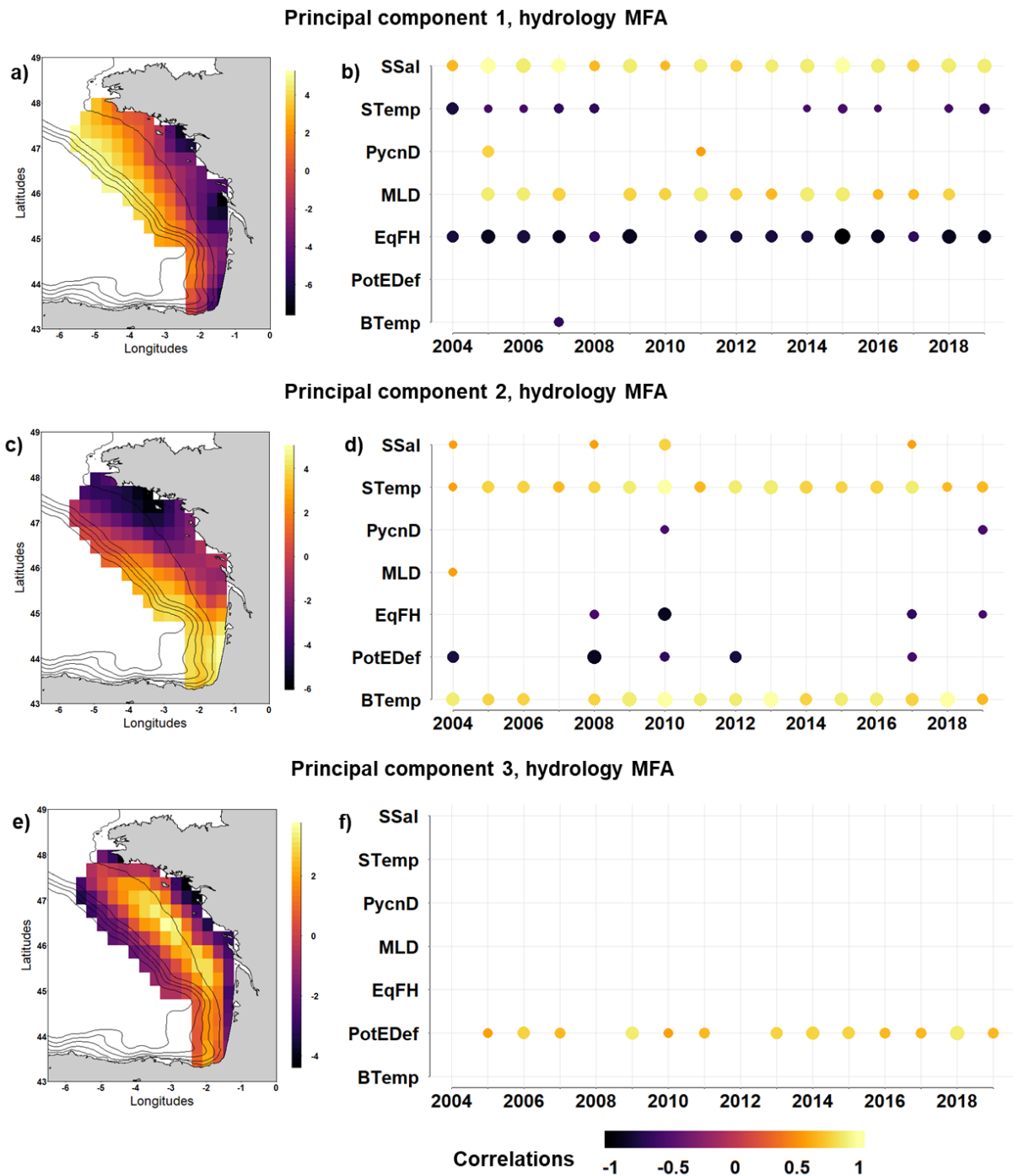


Fig. 10: Maps of mean individuals' (grid cells') coordinates on hydrology Multiple Factor Analysis (MFA) principal component (*PC*) 1 (a), 2 (c) and 3 (e), and time series of significant correlations (> |0.5|) between the seven hydrological parameters and the MFA *PC.1* (b), *PC.2* (d) and *PC.3* (f). The disk radii are proportional to the absolute value of the correlation coefficient. The hydrology MFA was performed on the maps time series of seven hydrological parameters derived from PELGAS and satellite data, from 2004 to 2019 (Table 2).

552 3.4.2 Primary producers ecosystem component

553 Here we present the spatial patterns of the primary producers ecosystem
 554 component, based on the mapping of grid cells coordinates in the primary producers
 555 MFA factorial space (Fig. 11a). The variables best correlated with the MFA PCs are
 556 shown in Fig. 11b.

557 The phytoMFA1 exhibited a dominant coastal – offshore gradient. This structure
 558 was highlighted by the low values offshore, along the shelf break in the south of the
 559 BoB (Fig. 11a, darkest cells). High value were located in coastal areas, with highest
 560 values off the Loire estuary and to a lesser extent, off the Gironde and Adour estuaries
 561 (Fig. 11a, lightest cells). Surface chlorophyll-a concentrations of organisms larger than
 562 20 μm , total surface chlorophyll-a concentrations and satellite-derived chlorophyll-a
 563 concentrations were consistently positively correlated to phytoMFA1, showing highest
 564 values in coastal areas, especially in the Loire estuary, between 2009 and 2019 (Fig.
 565 11b). On the contrary, the depth of the chlorophyll maximum displayed negative
 566 correlations with phytoMFA1 approximately every other year, revealing higher values
 567 along the shelf break in the south and contributing significantly to the coastal-offshore
 568 gradient in 2009, 2011, 2013, 2015, 2016 and 2019 (Fig. 11b).

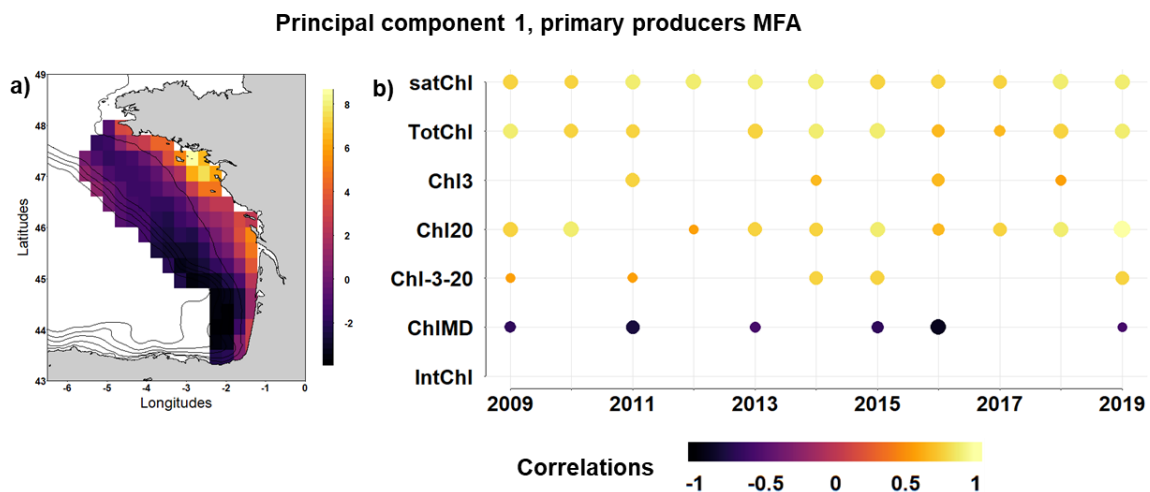


Fig. 11: Maps of mean individuals' (grid cells) coordinates on the primary producers Multiple Factor Analysis (MFA) principal component *PC.1* (a) and time series of significant correlations ($> |0.5|$) between the seven phytoplankton variables and *PC.1* (b). The disk radii are proportional to the absolute value of the correlation coefficient. The primary producers MFA was performed on the maps time series of chlorophyll-a parameters derived from PELGAS and satellite data, from 2009 to 2019 (Table 2).

569 3.4.3 *Small pelagic fish ecosystem component*

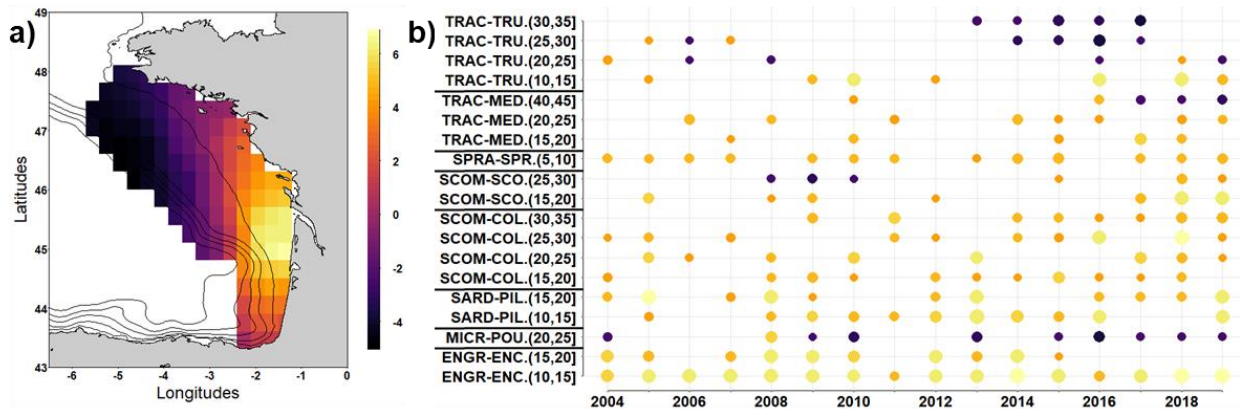
570 Here we present the spatial patterns of the SPF ecosystem component, based on
571 the mapping of grid cells coordinates in the SPF MFA factorial space (Fig. 12a). The
572 variables best correlated with the MFA *PCs* are shown in Fig. 12b.

573 The spfMFA1 map showed a south-eastern – north-western gradient. This structure
574 was underpinned by the lowest values offshore north to 45.5°N, along the shelf break
575 (Fig. 12a, darkest cells), and the highest in the south-eastern part, from the Gironde
576 estuary to 44.5°N (Fig. 12a, lightest cells). Small anchovy (*i.e.* ENGR-ENC. (10-15)),
577 sardine (*i.e.* SARD-PIL.), sprat (*i.e.* SPRA-SPR.) and Atlantic chub mackerel (*i.e.*
578 SCOM-COL.) of all sizes were positively correlated to spfMFA1 (Fig. 12b), displaying
579 higher biomass in the south-eastern part of the BoB. Note this pattern is particularly
580 consistent for large Atlantic chub mackerel after 2013 (six consecutive years for > 30
581 cm Atlantic chub mackerel). On the other hand, high biomass of blue whiting (*i.e.*
582 MICR-POU) and large Atlantic horse mackerel (*i.e.* TRAC-TRU > 25 cm) were found
583 offshore in the northern part of the BoB, showing negative correlations with spfMFA1,
584 at the end of the time series (after 2014 and between 2013 and 2017, respectively)
585 (Fig. 12b).

586 The spfMFA2 map showed an East – West gradient. This structure was underpinned
587 by the low values in the coastal area, from 46°N to 47.5°N, including the Brittany
588 southern coast (Fig. 12c, darkest cells), and high values in the southern part of the
589 BoB and along the shelf break, south to 46°N (Fig. 12c, lightest cells). Sprat between
590 10 and 15 cm (*i.e.* SPRA-SPR. (10-15)) had consistent negative correlations with the
591 spfMFA2, meaning that they had higher biomass in coastal areas. On the contrary,
592 large Atlantic mackerel (> 30 cm) (*i.e.* SCOM-COL.) had positive correlations with the
593 spfMFA2, showing higher biomass in the south. The same pattern was observed for
594 large Atlantic chub mackerel before 2013 (Fig. 12d).

595

Principal component 1, small pelagic fish MFA



Principal component 2, small pelagic fish MFA

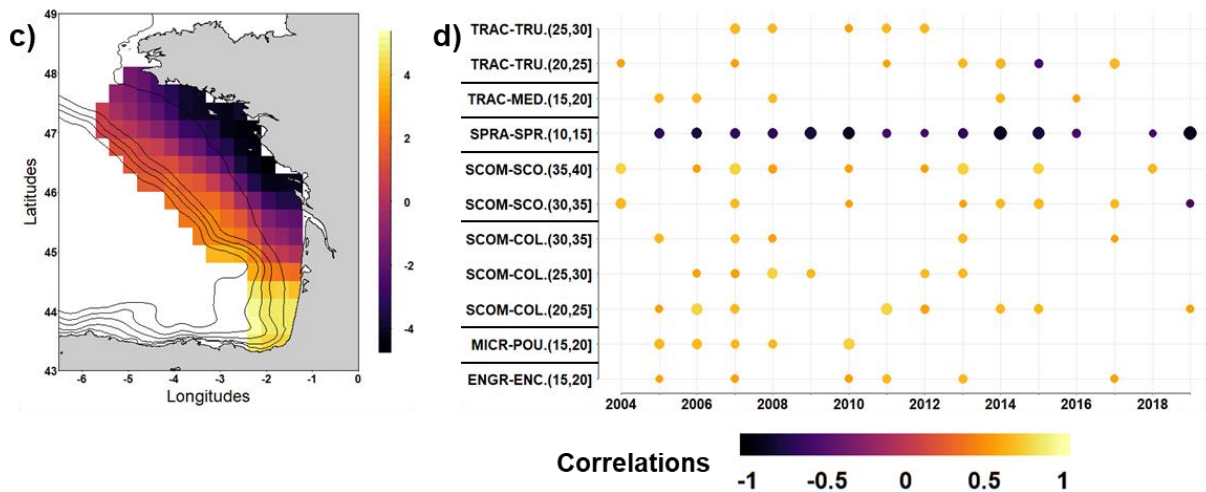


Fig. 12: Maps of mean individuals (grid cells) coordinates on small pelagic fish (SPF) Multiple Factor Analysis (MFA) principal component PC.1 (a) and PC.2 (c), and time series of significant correlations (> |0.5|) between the SPF species considered by 5 cm size classes and MFA PC.1 (b) and PC.2 (d). The disk radii are proportional to the absolute value of the correlation coefficient. The small pelagic fish MFA was performed on the maps time series of SPF species biomass considered by 5 cm size classes, calculated from the PELGAS data, from 2004 to 2019 (Table 3).

596 3.5 Correlates of the observed mesozooplankton space-time 597 patterns

598 We searched for correlates of the mesozooplankton main space-time patterns
599 (zooMFA1 and zooMFA2) using GLMs. We used the six selected *PCs* in the hydrology,
600 primary producers and SPF MFA as predictors.

601 *3.5.1 First PC in the mesozooplankton space-time pattern: zooMFA1*

602 For the initial full model built with the six predictors, all the VIF values were higher
 603 than five (except that of hydroMFA3, VIF value = 3.7), showing collinearity between all
 604 the predictors except hydroMFA3 (Appendix C, Table C.1). The predictors phytoMFA1
 605 and spfMFA2 had highest linear correlation coefficient with the other predictors
 606 (Appendix C, Fig. C.1) and were thus removed from the initial full model. The model
 607 without these two predictors showed acceptable VIF values and thus the predictors
 608 hydroMFA1, hydroMFA2, hydroMFA3 and spfMFA1 were kept for the subsequent
 609 model selection procedure.

610 The stepwise backward model selection procedure showed that the four
 611 predictors together constituted the best model explaining the zooMFA1 (lowest AIC,
 612 Appendix C, Table C.2). The salinity and water column stratification gradient
 613 (hydroMFA1, Fig. 5a and b) explained most of the variance in the model. To a lesser
 614 extent, the North - South gradient in the water temperature (hydroMFA2, Fig. 5c and
 615 d) and SPF biomass spatial patterns (spfMFA1, Fig. 12a and b) were also significant
 616 contributors explaining the mesozooplankton coastal-offshore gradient (zooMFA1, Fig.
 617 8a and b) (Table 4). On the other hand, the potential energy deficit spatial pattern
 618 (hydroMFA3, Fig. 5e and f) was not significant in the model (Table 4), but a model
 619 without this predictor was not significantly different from the best model, as their AIC
 620 difference was smaller than two (Appendix C, Table C.2).

621 Table 4: Predictors included in the model explaining the first principal component of the
 622 mesozooplankton MFA, with the estimated coefficients (“Estimate” and “Std. Error”) and their
 623 significance in the model (“P value”).

Parameters	Estimate	Std. Error	P value
(Intercept)	2.49	0.17	< 2e-16 ***
hydroMFA1	-0.093	0.015	4.88e-09 ***
hydroMFA2	-0.047	0.009	2.55e-06 ***
hydroMFA3	-0.023	0.012	0.07
spfMFA1	0.088	0.015	8.79e-08 ***

624

625 3.5.2 Second PC in the mesozooplankton space-time pattern: zooMFA2

626 Using the same procedure as previously (VIF value of the predictors in the initial
627 full model and correlation coefficients among predictors, see Appendix C, Table C.1
628 and Fig. C.1), the predictors hydroMFA1, phytoMFA1 and spfMFA2 were removed
629 from the analysis.

630 The stepwise backward model selection procedure was applied with the three
631 selected predictors (*i.e.* hydroMFA2, hydroMFA3 and spfMFA1). The best model
632 explaining zooMFA2 included hydroMFA2 and spfMFA1 (lowest AIC, Appendix C,
633 Table C.3) but hydroMFA2 as the only significant predictor (Table 5). The map of
634 zooMFA2 was underpinned by the North – South gradient in the biomass of
635 meroplanktonic crustaceans larvae (zooMFA2, Fig. 8c and d). Thus, this structuration
636 followed the North – South gradient in water temperature (hydroMFA2, Fig. 5c and d).
637 Both predictors hydroMFA3 and spfMFA1 were not significantly explicative in the
638 model (Table 5), but models without those predictors were not significantly different,
639 as their AIC difference was smaller than two (Appendix C, Table C.3). This suggested
640 that the potential energy deficit (hydroMFA3) and the SPF biomass spatial patterns
641 (spfMFA1) were less influential in structuring in the mesozooplankton North – South
642 gradient (zooMFA2).

643 Table 5: Predictors included in the model explaining the second principal component of the
644 mesozooplankton MFA, with the estimated coefficients (“Estimate” and “Std. Error”) and their
645 significance in the model (“P value”).

Parameters	Estimate	Std. Error	P value
(Intercept)	2.35	0.063	< 2e-16 ***
hydroMFA2	-0.13	0.006	< 2e-16 ***
hydroMFA3	0.007	0.009	0.434
spfMFA1	-0.008	0.005	0.113

646

647 **4 Discussion**

648 This study is the first space-time characterisation of mesozooplankton springtime
649 assemblages, over the BoB continental shelf and almost two decades. Results show
650 that the spatial patterns in the mesozooplankton assemblage was coherent with that
651 observed in other pelagic ecosystem components (hydrology, primary producers and
652 small pelagic fish). Coastal-offshore and North-South gradients were the main
653 mesoscale spatial patterns. Small copepods, gelatinous and meroplanktonic
654 organisms characterised coastal areas. Euchaetidae and meroplanktonic crustaceans'
655 larvae showed higher biomass in the northern part of the BoB while Metridinidae,
656 Cladocera, Appendicularia and Echinodermata had higher biomass in the southern
657 part. Moreover, the high correlations between the years and the mesozooplankton
658 MFA *PCs* underlined the stability in time of the above-mentioned spatial patterns. The
659 high occurrence frequencies of grid cells to the clusters defining specific regions in the
660 BoB evidenced the temporal consistency of the mesozooplankton assemblage spatial
661 structure. In the other pelagic ecosystem components taken into account, salinity,
662 water column stratification and primary producers supported a coastal-offshore
663 gradient, while surface and bottom water temperature drew a North-South gradient. In
664 addition, the spatial structure in the SPF biomass by size classes obtained here was
665 consistent with that obtained by Doray et al. (2018) with a similar methodology. Finally,
666 the observed mesozooplankton patterns were correlated with those of hydrology and
667 SPF ecosystem components.

668 **4.1 Mesozooplankton assemblages temporal stability**

669 The highest inter-annual variability occurred offshore in the northern part of the BoB,
670 where some grid cells had missing data at the beginning of the time series. Therefore,
671 this result can be due to the missing data imputation in this area. Yet, a true biological
672 variability in the mesozooplankton assemblage could also be real close to the shelf
673 break. The consistency in time of the mesozooplankton assemblage was a conclusion
674 drawn by Irigoien et al. (2008), studying spring zooplankton distribution between 1998
675 and 2006 in the southern part of the BoB. Feuilloley et al. (2022) also showed the high
676 stability through time of the zooplankton density, body size and taxonomic composition
677 in the North Western Mediterranean Sea, during the period 1995-2019. Yet, abrupt

678 shifts in community structure could be expected when analysing long-term dynamics
679 in the context of environmental changes. Such regime shifts were detected in the late
680 1980s and in the 1990s in several marine regions in the Northern Hemisphere
681 (Beaugrand et al., 2015; Morse et al., 2017; Bode et al., 2020; Chust et al., 2022).
682 Recently, Dessier et al. (2018) found a change in the large copepod species
683 dominance in the South of the BoB between the period 2003 – 2006 and the period
684 2007 – 2009, preceding a return toward the initial situation over the period 2010 –
685 2013. Also, Iriarte et al. (2022) distinguished three periods in the relative density of
686 copepod species in the Southeastern BoB: 1998 – 2007, 2008 – 2013 and 2014 –
687 2015. Here, the mesozooplankton community was studied using 24 taxonomic groups,
688 a less detailed level than the species level used in these previous studies. Fine
689 taxonomic resolution could reveal shifts in species dominance that could compensate
690 each other when analysing the community at a broader taxonomic resolution and,
691 consequently, the overall structure could appear consistent in time. This point
692 constitutes a potential limit of our study. Shifts in species dominance could have
693 occurred in the zooplankton community between 2004 and 2019 but the broad
694 taxonomic resolution used here may not have enable the observation of such possible
695 changes, resulting in an apparent temporal stability over the time series. On the other
696 hand, these studies were done at a smaller spatial scale (southern part of the BoB in
697 Dessier et al. (2018); two neritic stations in the Cantabrian Sea in Iriarte et al. (2022)),
698 and the shifts occurring in restricted areas could be undetectable at a broader spatial
699 scale or not affect the large scale distribution pattern.

700 **4.2 Coherent spatial patterns across pelagic ecosystem** 701 **components**

702 Our results agreed with the spatial organisation in mesozooplankton assemblages
703 along a coastal-offshore gradient previously showed in the BoB (Albaina and Irigoien,
704 2004, 2007a; Sourisseau and Carlotti, 2006; Irigoien et al., 2008; Vandromme et al.,
705 2014; Dessier et al., 2018) and in other shelf ecosystems (Marcolin et al., 2013; Pepin
706 et al., 2015; Noyon et al., 2022). Our study also confirms that surface and bottom water
707 temperature, salinity-related parameters and water column stratification indices were
708 key hydrographic variables that correlated with this mesozooplankton springtime
709 spatial structure (Albaina and Irigoien, 2004; Zarauz et al., 2007; Irigoien et al., 2011;

710 Dessier et al., 2018; Iriarte et al., 2022). Hydrological parameters integrating the
711 historical seasonal conditions, such as the equivalent freshwater height, mixed layer
712 depth and the deficit of potential energy, were key variables to study the
713 mesozooplankton spring habitat, taking into account the onset of spring conditions.
714 The correlations between the hydrology and primary producers space-time patterns
715 observed here confirm the important role of nutrients enrichment at the rivers' mouths
716 in the primary producers development in spring in the BoB (Guillaud et al., 2008).
717 Primary producers are known to drive the mesozooplankton dynamics in the BoB
718 (Zarauz et al., 2008; Dessier et al., 2018; Iriarte et al., 2022) and elsewhere (Pepin et
719 al., 2015; Capuzzo et al., 2018). Here, because of the method used, the primary
720 producers' space-time pattern was not included in the models to explain the
721 mesozooplankton space-time structure. Yet, the correlations between the hydrology
722 and primary producers ecosystem components (Appendix C, Fig. C.1) combined with
723 the hydrology space-time patterns significance in the linear models (Tables 4 and 5)
724 suggest that the hydrological landscapes may influenced the mesozooplankton
725 community structure through the primary production and trophic relationships between
726 phytoplankton and mesozooplankton in the BoB.

727 The North-South gradient in the mesozooplankton assemblage in the BoB was
728 never described before, as previous studies mostly focused on the southern part of the
729 BoB (Albaina and Irigoien, 2004, 2007a; Irigoien et al., 2008; Dessier et al., 2018). At
730 the scale of the Northeast Atlantic, a strong latitudinal effect potentially driven by
731 temperature regimes has been shown on the seasonal and interannual variability of
732 two copepod species (Valdes et al., 2022). Moreover, Fanjul et al. (2019) demonstrated
733 that some zooplankton groups' abundances displayed temperature-mediated
734 latitudinal differences, and that meroplankton contributed more than holoplankton to
735 the main between-site differences. In the BoB, the spring meroplanktonic crustaceans'
736 larvae distribution could be driven by the temperature-induced latitudinal gradient,
737 resulting in higher biomass in the northern coastal area. Nevertheless, this result could
738 also highlight the timing of the surveys, lasting one month and starting in the south of
739 the BoB, potentially before the development of the meroplanktonic crustaceans' larvae
740 in this area.

741 Furthermore, the correlation between mesozooplankton and SPF spatial patterns
742 confirms the consistent spatial structure across pelagic ecosystem components that

743 have been reported in the BoB (Doray et al., 2018a; Petitgas et al., 2018), possibly
744 mediated via predation and/or forced by hydrological structuring. For example, taking
745 into account the eight major SPF species inhabiting the BoB, Bachiller and Irigoien
746 (2015) described an overall high diet overlap and concluded to a top – down control by
747 these planktivorous fishes on zooplankton. Elsewhere, such links between ecosystem
748 components were highlighted in the Mediterranean Sea (Feuilloley et al., 2020), on the
749 Portuguese continental coast (Fonseca et al., 2022), in the North Sea (Capuzzo et al.,
750 2018) and in Barents Sea (Stige et al., 2014). Here, the spatial structures in the
751 hydrological parameters, primary producers and SPF were similar to that in
752 mesozooplankton assemblages and were also consistent in time. Spatial structures
753 had been described for different ecosystem components in the BoB (Special Issue No.
754 166 in Progress in Oceanography, 2018), including river plumes, primary producers,
755 fish and top-predators but this is the first time they are described for the
756 mesozooplankton and shown to be similar to the other ecosystem components. Such
757 consistency in the spatial structure across ecosystem components and over time is
758 remarkable. Donohue et al. (2013) discussed the multiple and related facets of
759 ecosystem stability. In the case of the BoB continental shelf at springtime, hydrographic
760 landscapes resulting from river plumes' extents on the shelf and temperature gradients
761 (Koutsikopoulos and Le Cann, 1996; Koutsikopoulos et al., 1998; Castaing et al., 1999;
762 Planque et al., 2004; Guillaud et al., 2008) certainly impede strong structuring meso-
763 scale forcings on the BoB regional pelagic ecology. The structure could also be
764 maintained and reinforced by top-down and bottom-up controls through trophic levels
765 as generally reported for the North Atlantic (Frank et al., 2007) although not directly
766 studied here.

767 **4.3 Data and methods used**

768 Such regional study linking several ecological components was made possible by
769 the unique long-term and spatially resolved datasets constructed from integrated
770 surveys. Thus, maintaining such surveys is of primary importance for ecosystem
771 assessment research, especially in the context of climate change, as they provide a
772 platform dedicated to gather data from several biological and abiotic components at
773 the same temporal and spatial resolution (Kupschus et al., 2016; Doray et al., 2018c).
774 Nevertheless, it should be noted that these *in situ* data sets provide a temporal

775 snapshot of the ecosystem state at the time of the surveys. Any apparent interannual
776 variability could be caused by interannual differences in the seasonal evolution of the
777 system (Huret et al., 2018). The combination of imaging and deep learning tools
778 provided an efficient method to analyse a high quantity of mesozooplankton samples
779 quickly and in a standardized way. This analytical pipeline, including also automated
780 procedures for spatial gridding and missing data imputation, allowed to construct a
781 mesozooplankton spatially resolved time series over 16 years. Finally, the MFA was
782 well suited to estimate time-average spatial patterns in a multivariate dataset and
783 perhaps less designed to evidence temporal trends in the mean distribution, at least in
784 the way we implemented the method. Moreover, the results showing consistency in
785 time of the spatial patterns were based on a subset of MFA principal components,
786 accounting only for part of the total variance. The residual variance, not fully explained
787 here, showed exceptional events, which we did not fully explore. Yet, the major time
788 variations happened in particular years (for example, lowest mesozooplankton
789 biomass in 2011 and 2015, Fig. 3) and were located in particular areas (offshore in the
790 northern part of the BoB, Fig. 8), suggesting no obvious trend in time.

791 **5 Conclusion**

792 Thanks to long-term spatially resolved time series, we provided the first space-time
793 characterisation of mesozooplankton springtime assemblage, correlated with other
794 pelagic ecosystem components (hydrology, primary producers and SPF), over 16
795 years and the whole BoB continental shelf. We demonstrated coherent spatial patterns
796 across pelagic ecosystem components supported by coastal-offshore and North-South
797 gradients. Moreover, we highlighted the remarkable stability in time of these spatial
798 patterns. The springtime spatial structure of biotic components seems to be based on
799 spring hydrological landscapes and is potentially related to bottom-up and top-down
800 trophic controls, although a more detailed study on the ecosystem components'
801 correlations is needed to fully confirm this hypothesis. Our regional study relies on
802 long-term spatially resolved datasets originating from integrated surveys and provide
803 key understanding of the ecosystem structure and dynamics. Therefore, our work
804 emphasize the importance of such surveys for ecosystem assessment research
805 especially in the context of climate change.

806 **6 Acknowledgements**

807 The authors acknowledge receiving funding from the Ifremer DEFIPEL project
808 France Filière Pêche projet d'avenir. NG acknowledges being funded by Region Pays
809 de la Loire, FR and Ifremer. The authors wish to thanks the following technicians and
810 engineers for their decisive contribution to the sample and data acquisition: P. Pineau
811 (La Rochelle University), primary producers sampling and data acquisition; S. Le
812 Mestre (Ifremer), zooplankton sampling lab work on board and ZooCAM management
813 on land; P. Bourriau (Ifremer): zooplankton sampling and wet lab management on
814 board and on land; B. Forest (Ifremer), design and development of ZooCAM software;
815 A. Nowaczyk (PlanktonLab and University of Bordeaux) and the PIQV team (Sorbonne
816 Université – CNRS), expertise in zooplankton identification. The authors wish also to
817 thank the many other students, technicians and scientists who participated in the
818 sampling and samples management on board and on land, and the successive crews
819 of the R/V Thalassa involved in the PELGAS cruises from 2004 to 2019.

820 **7 Authors contributions**

821 NG: conceptualized the study, generated and scrutinized the imaging data, conducted
822 the numerical analyses, drafted the paper. J-BR: conceptualized the study, supervised
823 NG work, scrutinized the imaging data, drafted the paper. CD: conceptualized the
824 study, supervised NG work, drafted the paper. MD: supervised numerical analyses and
825 provided fish data, participated in the drafting. MH: provided hydrology data,
826 participated in the drafting. PP: conceptualized the study, supervised NG work, drafted
827 the paper. All co-authors reviewed and revised the paper before submission.

828

829 **8 References**

- 830 Abdi, H., Williams, L.J., Valentin, D., 2013. Multiple factor analysis: principal
831 component analysis for multitable and multiblock data sets: Multiple factor analysis.
832 Wiley Interdiscip. Rev. Comput. Stat. 5, 149–179. <https://doi.org/10.1002/wics.1246>
- 833 Albaina, A., Irigoien, X., 2007a. Fine scale zooplankton distribution in the Bay of Biscay
834 in spring 2004. J. Plankton Res. 29, 851–870. <https://doi.org/10.1093/plankt/fbm064>
- 835 Albaina, A., Irigoien, X., 2007b. Zooplankton communities and oceanographic
836 structures in a high-resolution grid in the south-eastern corner of the Bay of Biscay.
837 Estuar. Coast. Shelf Sci. 75, 433–446. <https://doi.org/10.1016/j.ecss.2007.05.028>
- 838 Albaina, A., Irigoien, X., 2004. Relationships between frontal structures and
839 zooplankton communities along a cross-shelf transect in the Bay of Biscay (1995 to
840 2003). Mar. Ecol. Prog. Ser. 284, 65–75. <https://doi.org/10.3354/meps284065>
- 841 Bachiller, E., Irigoien, X., 2015. Trophodynamics and diet overlap of small pelagic fish
842 species in the Bay of Biscay. Mar. Ecol. Prog. Ser. 534, 179–198.
843 <https://doi.org/10.3354/meps11375>
- 844 Banse, K., 1995. Zooplankton: Pivotal role in the control of ocean production: I.
845 Biomass and production. ICES J. Mar. Sci. 52, 265–277. [https://doi.org/10.1016/1054-3139\(95\)80043-3](https://doi.org/10.1016/1054-3139(95)80043-3)
- 847 Batchelder, H.P., Mackas, D.L., O'Brien, T.D., 2012. Spatial–temporal scales of
848 synchrony in marine zooplankton biomass and abundance patterns: A world-wide
849 comparison. Prog. Oceanogr. 97–100, 15–30.
850 <https://doi.org/10.1016/j.pocean.2011.11.010>
- 851 Beaugrand, G., Conversi, A., Chiba, S., Edwards, M., Fonda-Umani, S., Greene, C.,
852 Mantua, N., Otto, S.A., Reid, P.C., Stachura, M.M., Stemmann, L., Sugisaki, H., 2015.
853 Synchronous marine pelagic regime shifts in the Northern Hemisphere. Philos. Trans.
854 R. Soc. B Biol. Sci. 370, 20130272. <https://doi.org/10.1098/rstb.2013.0272>
- 855 Bellier, E., Planque, B., Petitgas, P., 2007. Historical fluctuations in spawning location
856 of anchovy (*Engraulis encrasicolus*) and sardine (*Sardina pilchardus*) in the Bay of
857 Biscay during 1967–73 and 2000–2004. Fish. Oceanogr. 16, 1–15.
858 <https://doi.org/10.1111/j.1365-2419.2006.00410.x>

859 Bode, A., Álvarez, M., García García, L.M., Louro, M.Á., Nieto-Cid, M., Ruíz-Villarreal,
860 M., Varela, M.M., 2020. Climate and Local Hydrography Underlie Recent Regime
861 Shifts in Plankton Communities off Galicia (NW Spain). *Oceans* 1, 181–197.
862 <https://doi.org/10.3390/oceans1040014>

863 Burnham, K.P., Anderson, D.R., Burnham, K.P., 2002. Model selection and multimodel
864 inference: a practical information-theoretic approach, 2nd ed. ed. Springer, New York.

865 Capuzzo, E., Lynam, C.P., Barry, J., Stephens, D., Forster, R.M., Greenwood, N.,
866 McQuatters-Gollop, A., Silva, T., van Leeuwen, S.M., Engelhard, G.H., 2018. A decline
867 in primary production in the North Sea over 25 years, associated with reductions in
868 zooplankton abundance and fish stock recruitment. *Glob. Change Biol.* 24, e352–e364.
869 <https://doi.org/10.1111/gcb.13916>

870 Castaing, P., Froidefond, J.M., Lazure, P., Weber, O., Prud'homme, R., Jouanneau,
871 J.M., 1999. Relationship between hydrology and seasonal distribution of suspended
872 sediments on the continental shelf of the Bay of Biscay. *Deep Sea Res. Part II Top.*
873 *Stud. Oceanogr.* 46, 1979–2001. [https://doi.org/10.1016/S0967-0645\(99\)00052-1](https://doi.org/10.1016/S0967-0645(99)00052-1)

874 Charrad, M., Ghazzali, N., Boiteau, V., Niknafs, A., 2014. NbClust: An R Package for
875 Determining the Relevant Number of Clusters in a Data Set. *J. Stat. Softw.* 61, 1–36.
876 <https://doi.org/10.18637/jss.v061.i06>

877 Chust, G., González, M., Fontán, A., Revilla, M., Alvarez, P., Santos, M., Cotano, U.,
878 Chifflet, M., Borja, A., Muxika, I., Sagarminaga, Y., Caballero, A., de Santiago, I.,
879 Epelde, I., Liria, P., Ibaibarriaga, L., Garnier, R., Franco, J., Villarino, E., Irigoien, X.,
880 Fernandes-Salvador, J.A., Uriarte, Andrés, Esteban, X., Orue-Echevarria, D., Figueira,
881 T., Uriarte, Adolfo, 2022. Climate regime shifts and biodiversity redistribution in the Bay
882 of Biscay. *Sci. Total Environ.* 803, 149622.
883 <https://doi.org/10.1016/j.scitotenv.2021.149622>

884 Colas, F., Tardivel, M., Perchoc, J., Lunven, M., Forest, B., Guyader, G., Danielou,
885 M.M., Le Mestre, S., Bourriau, P., Antajan, E., Sourisseau, M., Huret, M., Petitgas, P.,
886 Romagnan, J.B., 2018. The ZooCAM, a new in-flow imaging system for fast onboard
887 counting, sizing and classification of fish eggs and metazooplankton. *Prog. Oceanogr.*,
888 *Multidisciplinary integrated surveys* 166, 54–65.
889 <https://doi.org/10.1016/j.pocean.2017.10.014>

890 Cury, P., Bakun, A., Crawford, R.J.M., Jarre, A., Quiñones, R.A., Shannon, L.J.,
891 Verheye, H.M., 2000. Small pelagics in upwelling systems: patterns of interaction and
892 structural changes in “wasp-waist” ecosystems. *ICES J. Mar. Sci.* 57, 603–618.
893 <https://doi.org/10.1006/jmsc.2000.0712>

894 Dessier, A., Bustamante, P., Chouvelon, T., Huret, M., Pagano, M., Marquis, E.,
895 Rousseaux, F., Pignon-Mussaud, C., Mornet, F., Bréret, M., Dupuy, C., 2018. The
896 spring mesozooplankton variability and its relationship with hydrobiological structure
897 over year-to-year changes (2003–2013) in the southern Bay of Biscay (Northeast
898 Atlantic). *Prog. Oceanogr., Multidisciplinary integrated surveys* 166, 76–87.
899 <https://doi.org/10.1016/j.pocean.2018.04.011>

900 Donohue, I., Petchey, O.L., Montoya, J.M., Jackson, A.L., McNally, L., Viana, M.,
901 Healy, K., Lurgi, M., O’Connor, N.E., Emmerson, M.C., 2013. On the dimensionality of
902 ecological stability. *Ecol. Lett.* 16, 421–429. <https://doi.org/10.1111/ele.12086>

903 Doray, M., Boyra, G., van der Kooij, J., 2021. ICES Survey Protocols - Manual for
904 acoustic surveys coordinated under ICES Working Group on Acoustic and Egg
905 Surveys for Small Pelagic Fish (WGACEGG).
906 <https://doi.org/10.17895/ICES.PUB.7462>

907 Doray, M., Duhamel, E., Boiron-Leroy, A., Marchand, L., Bled--Defruit, G., Petitgas, P.,
908 2022. Mean length and weight at-age of anchovy and sardine estimated during the
909 PELGAS survey in the Bay of Biscay in springtime. <https://doi.org/10.17882/88357>

910 Doray, M., Hervy, C., Huret, M., Petitgas, P., 2018a. Spring habitats of small pelagic
911 fish communities in the Bay of Biscay. *Prog. Oceanogr., Multidisciplinary integrated*
912 *surveys* 166, 88–108. <https://doi.org/10.1016/j.pocean.2017.11.003>

913 Doray, M., Petitgas, P., Huret, M., Duhamel, E., Romagnan, J.B., Authier, M., Dupuy,
914 C., Spitz, J., 2018b. Monitoring small pelagic fish in the Bay of Biscay ecosystem, using
915 indicators from an integrated survey. *Prog. Oceanogr., Multidisciplinary integrated*
916 *surveys* 166, 168–188. <https://doi.org/10.1016/j.pocean.2017.12.004>

917 Doray, M., Petitgas, P., Romagnan, J.B., Huret, M., Duhamel, E., Dupuy, C., Spitz, J.,
918 Authier, M., Sanchez, F., Berger, L., Dorémus, G., Bourriau, P., Grellier, P., Massé, J.,
919 2018c. The PELGAS survey: Ship-based integrated monitoring of the Bay of Biscay

920 pelagic ecosystem. *Prog. Oceanogr.*, Multidisciplinary integrated surveys 166, 15–29.
921 <https://doi.org/10.1016/j.pocean.2017.09.015>

922 Doray, M., Petitgas, P., Saraux, C., Cornou, A.-S., 2013. EchoR: R Package for
923 Computing Indices of the State of Fish Population and Communities, based on
924 Fisheries Acoustic Data, R Package. *Ifremer* 10.

925 Escofier, B., Pagès, J., 1994. Multiple factor analysis (AFMULT package). *Comput.*
926 *Stat. Data Anal.* 18, 121–140. [https://doi.org/10.1016/0167-9473\(94\)90135-X](https://doi.org/10.1016/0167-9473(94)90135-X)

927 Fanjul, A., Iriarte, A., Villate, F., Uriarte, I., Artiach, M., Atkinson, A., Cook, K., 2019.
928 Latitude, distance offshore and local environmental features as modulators of
929 zooplankton assemblages across the NE Atlantic Shelves Province. *J. Plankton Res.*
930 41, 293–308. <https://doi.org/10.1093/plankt/fbz015>

931 Feuilleley, G., Fromentin, J.-M., Saraux, C., Irisson, J.-O., Jalabert, L., Stemmann, L.,
932 2022. Temporal fluctuations in zooplankton size, abundance, and taxonomic
933 composition since 1995 in the North Western Mediterranean Sea. *ICES J. Mar. Sci.*
934 79, 882–900. <https://doi.org/10.1093/icesjms/fsab190>

935 Feuilleley, G., Fromentin, J.-M., Stemmann, L., Demarcq, H., Estournel, C., Saraux,
936 C., 2020. Concomitant changes in the environment and small pelagic fish community
937 of the Gulf of Lions. *Prog. Oceanogr.* 186, 102375.
938 <https://doi.org/10.1016/j.pocean.2020.102375>

939 Fonseca, P., Silva, A.D., Angélico, M.M., Garrido, S., 2022. Seasonal and spatial
940 variability of Atlanto-Iberian pelagic fish diet with estimates of intraguild predation. *Mar.*
941 *Ecol. Prog. Ser.* 687, 95–111. <https://doi.org/10.3354/meps14011>

942 Fox, J., Monette, G., 1992. Generalized Collinearity Diagnostics. *J. Am. Stat. Assoc.*
943 87, 178–183. <https://doi.org/10.1080/01621459.1992.10475190>

944 Fox, J., Weisberg, S., 2019. *An R Companion to Applied Regression*. Sage Thousand
945 Oaks CA Third Edition.

946 Frank, K.T., Petrie, B., Shackell, N.L., 2007. The ups and downs of trophic control in
947 continental shelf ecosystems. *Trends Ecol. Evol.* 22, 236–242.
948 <https://doi.org/10.1016/j.tree.2007.03.002>

949 Garcia-Herrera, N., Cornils, A., Laudien, J., Niehoff, B., Höfer, J., Försterra, G.,
950 González, H.E., Richter, C., 2022. Seasonal and diel variations in the vertical
951 distribution, composition, abundance and biomass of zooplankton in a deep Chilean
952 Patagonian Fjord. *PeerJ* 10, e12823. <https://doi.org/10.7717/peerj.12823>

953 Garijo, J.C., Hernández-León, S., 2015. The use of an image-based approach for the
954 assessment of zooplankton physiological rates: a comparison with enzymatic methods.
955 *J. Plankton Res.* 37, 923–938. <https://doi.org/10.1093/plankt/fbv056>

956 Giering, S.L.C., Wells, S.R., Mayers, K.M.J., Schuster, H., Cornwell, L., Fileman, E.S.,
957 Atkinson, A., Cook, K.B., Preece, C., Mayor, D.J., 2019. Seasonal variation of
958 zooplankton community structure and trophic position in the Celtic Sea: A stable
959 isotope and biovolume spectrum approach. *Prog. Oceanogr., Shelf Sea*
960 *Biogeochemistry: Pelagic Processes.* 177, 101943.
961 <https://doi.org/10.1016/j.pocean.2018.03.012>

962 Gohin, F., 2011. Annual cycles of chlorophyll-a, non-algal suspended particulate
963 matter, and turbidity observed from space and in-situ in coastal waters. *Ocean Sci.* 7,
964 705–732. <https://doi.org/10.5194/os-7-705-2011>

965 González-Gil, R., Taboada, F.G., Höfer, J., Anadón, R., 2015. Winter mixing and
966 coastal upwelling drive long-term changes in zooplankton in the Bay of Biscay (1993–
967 2010). *J. Plankton Res.* 37, 337–351. <https://doi.org/10.1093/plankt/fbv001>

968 Gorsky, G., Ohman, M.D., Picheral, M., Gasparini, S., Stemmann, L., Romagnan, J.-
969 B., Cawood, A., Pesant, S., García-Comas, C., Prejger, F., 2010. Digital zooplankton
970 image analysis using the ZooScan integrated system. *J. Plankton Res.* 32, 285–303.
971 <https://doi.org/10.1093/plankt/fbp124>

972 Guillaud, J.-F., Aminot, A., Delmas, D., Gohin, F., Lunven, M., Labry, C., Herbland, A.,
973 2008. Seasonal variation of riverine nutrient inputs in the northern Bay of Biscay
974 (France), and patterns of marine phytoplankton response. *J. Mar. Syst., Oceanography*
975 *of the Bay of Biscay* 72, 309–319. <https://doi.org/10.1016/j.jmarsys.2007.03.010>

976 Hays, G., Richardson, A., Robinson, C., 2005. Climate change and marine plankton.
977 *Trends Ecol. Evol.* 20, 337–344. <https://doi.org/10.1016/j.tree.2005.03.004>

978 Hernández-León, S., Koppelman, R., Fraile-Nuez, E., Bode, A., Mompeán, C.,
979 Irigoien, X., Olivar, M.P., Echevarría, F., Fernández de Puelles, M.L., González-

980 Gordillo, J.I., Cózar, A., Acuña, J.L., Agustí, S., Duarte, C.M., 2020. Large deep-sea
981 zooplankton biomass mirrors primary production in the global ocean. *Nat. Commun.*
982 11, 6048. <https://doi.org/10.1038/s41467-020-19875-7>

983 Huret, M., Bourriau, P., Doray, M., Gohin, F., Petitgas, P., 2018. Survey timing vs.
984 ecosystem scheduling: Degree-days to underpin observed interannual variability in
985 marine ecosystems. *Prog. Oceanogr.* 166, 30–40.
986 <https://doi.org/10.1016/j.pocean.2017.07.007>

987 Huret, M., Sourisseau, M., Petitgas, P., Struski, C., Léger, F., Lazure, P., 2013. A multi-
988 decadal hindcast of a physical–biogeochemical model and derived oceanographic
989 indices in the Bay of Biscay. *J. Mar. Syst.* 109–110, S77–S94.
990 <https://doi.org/10.1016/j.jmarsys.2012.02.009>

991 ICES, 2010. Life-cycle spatial patterns of small pelagic fish in the Northeast Atlantic.
992 ICES Coop. Res. Rep. 98.

993 Iriarte, A., Villate, F., Uriarte, I., Bidegain, G., Barroeta, Z., 2022. Shifts in neritic
994 copepod communities off the Basque coast (southeastern Bay of Biscay) between
995 1998 and 2015. *ICES J. Mar. Sci.* 79, 830–843.
996 <https://doi.org/10.1093/icesjms/fsab265>

997 Irigoien, X., Chust, G., Antonio Fernandes, J., Albaina, A., Zarauz, L., 2011. Factors
998 determining the distribution and beta diversity of mesozooplankton species in shelf and
999 coastal waters of the Bay of Biscay. *J. Plankton Res.* 33, 1182–1192.
1000 <https://doi.org/10.1093/plankt/fbr026>

1001 Irigoien, X., Fernandes, J.A., Grosjean, P., Denis, K., Albaina, A., Santos, M., 2008.
1002 Spring zooplankton distribution in the Bay of Biscay from 1998 to 2006 in relation with
1003 anchovy recruitment. *J. Plankton Res.* 31, 1–17. <https://doi.org/10.1093/plankt/fbn096>

1004 Josse, J., Husson, F., 2016. missMDA : A Package for Handling Missing Values in
1005 Multivariate Data Analysis. *J. Stat. Softw.* 70. <https://doi.org/10.18637/jss.v070.i01>

1006 Kerkar, A.U., Venkataramana, V., Tripathy, S.C., 2022. Assessing the trophic link
1007 between primary and secondary producers in the Southern Ocean: A carbon-biomass
1008 based approach. *Polar Sci.* 31, 100734. <https://doi.org/10.1016/j.polar.2021.100734>

1009 Koutsikopoulos, C., Beillois, P., Leroy, C., Taillefer, F., 1998. Temporal trends and
1010 spatial structures of the sea surface temperature in the Bay of Biscay. *Oceanol. Acta*
1011 21, 335–344. [https://doi.org/10.1016/S0399-1784\(98\)80020-0](https://doi.org/10.1016/S0399-1784(98)80020-0)

1012 Koutsikopoulos, C., Le Cann, B., 1996. Physical processes and hydrological structures
1013 related to the Bay of Biscay anchovy. *Sci. Mar.* 9–19.

1014 Kupschus, S., Schratzberger, M., Righton, D., 2016. Practical implementation of
1015 ecosystem monitoring for the ecosystem approach to management. *J. Appl. Ecol.* 53,
1016 1236–1247. <https://doi.org/10.1111/1365-2664.12648>

1017 Lê, S., Josse, J., Husson, F., 2008. FactoMineR: An R Package for Multivariate
1018 Analysis. *J. Stat. Softw.* 25, 1–18. <https://doi.org/10.18637/jss.v025.i01>

1019 Lehette, P., Hernández-León, S., 2009. Zooplankton biomass estimation from digitized
1020 images: a comparison between subtropical and Antarctic organisms: Zooplankton
1021 biomass by digital images. *Limnol. Oceanogr. Methods* 7, 304–308.
1022 <https://doi.org/10.4319/lom.2009.7.304>

1023 Makhlouf Belkahia, N., Pagano, M., Chevalier, C., Devenon, J.L., Daly Yahia, M.N.,
1024 2021. Zooplankton abundance and community structure driven by tidal currents in a
1025 Mediterranean coastal lagoon (Boughrara, Tunisia, SW Mediterranean Sea). *Estuar.*
1026 *Coast. Shelf Sci.* 250, 107101. <https://doi.org/10.1016/j.ecss.2020.107101>

1027 Marcolin, C. da R., Schultes, S., Jackson, G.A., Lopes, R.M., 2013. Plankton and
1028 seston size spectra estimated by the LOPC and ZooScan in the Abrolhos Bank
1029 ecosystem (SE Atlantic). *Cont. Shelf Res.* 70, 74–87.
1030 <https://doi.org/10.1016/j.csr.2013.09.022>

1031 Marcolin, C.R., Gaeta, S., Lopes, R.M., 2015. Seasonal and interannual variability of
1032 zooplankton vertical distribution and biomass size spectra off Ubatuba, Brazil. *J.*
1033 *Plankton Res.* 37, 808–819. <https://doi.org/10.1093/plankt/fbv035>

1034 Masse, J., Uriarte, A., Angelico, M., Carrera, P., 2018. Pelagic survey series for sardine
1035 and anchovy in ICES subareas 8 and 9 — Towards an ecosystem approach. *ICES*
1036 *Coop. Res. Rep.* <https://doi.org/10.17895/ices.pub.4599>

1037 Mitra, A., Davis, C., 2010. Defining the “to” in end-to-end models. *Prog. Oceanogr.*,
1038 Special Issue: Parameterisation of Trophic Interactions in Ecosystem Modelling 84,
1039 39–42. <https://doi.org/10.1016/j.pocean.2009.09.004>

1040 Morse, R.E., Friedland, K.D., Tommasi, D., Stock, C., Nye, J., 2017. Distinct
1041 zooplankton regime shift patterns across ecoregions of the U.S. Northeast continental
1042 shelf Large Marine Ecosystem. *J. Mar. Syst.* 165, 77–91.
1043 <https://doi.org/10.1016/j.jmarsys.2016.09.011>

1044 Noyon, M., Poulton, A.J., Asdar, S., Weitz, R., Giering, S.L.C., 2022. Mesozooplankton
1045 community distribution on the Agulhas Bank in autumn: Size structure and production
1046 | Elsevier Enhanced Reader. *Deep-Sea Part II* 195.
1047 <https://doi.org/10.1016/j.dsr2.2021.105015>

1048 Pagès, J., 2014. Multiple Factor Analysis by Example Using R, 1st ed. Chapman and
1049 Hall/CRC. <https://doi.org/10.1201/b17700>

1050 Pepin, P., Johnson, C.L., Harvey, M., Casault, B., Chassé, J., Colbourne, E.B.,
1051 Galbraith, P.S., Hebert, D., Lazin, G., Maillet, G., Plourde, S., Starr, M., 2015. A
1052 multivariate evaluation of environmental effects on zooplankton community structure
1053 in the western North Atlantic. *Prog. Oceanogr.* 134, 197–220.
1054 <https://doi.org/10.1016/j.pocean.2015.01.017>

1055 Petitgas, P., Doray, M., Huret, M., Massé, J., Woillez, M., 2014. Modelling the variability
1056 in fish spatial distributions over time with empirical orthogonal functions: anchovy in
1057 the Bay of Biscay. *ICES J. Mar. Sci.* 71, 2379–2389.
1058 <https://doi.org/10.1093/icesjms/fsu111>

1059 Petitgas, P., Goarant, A., Massé, J., Bourriau, P., 2009. Combining acoustic and
1060 CUFES data for the quality control of fish-stock survey estimates. *ICES J. Mar. Sci.*
1061 66, 1384–1390. <https://doi.org/10.1093/icesjms/fsp007>

1062 Petitgas, P., Huret, M., Dupuy, C., Spitz, J., Authier, M., Romagnan, J.B., Doray, M.,
1063 2018. Ecosystem spatial structure revealed by integrated survey data. *Prog.*
1064 *Oceanogr.*, Multidisciplinary integrated surveys 166, 189–198.
1065 <https://doi.org/10.1016/j.pocean.2017.09.012>

1066 Picheral, M., Colin, S., Irisson, J.O., 2017. EcoTaxa, a tool for the taxonomic
1067 classification of images. URL [Httpecotaxa Obs-Vlfr Fr](http://Httpecotaxa.Obs-Vlfr.Fr).

1068 Planque, B., Lazure, P., Jégou, A.-M., 2004. Detecting hydrological landscapes over
1069 the Bay of Biscay continental shelf in spring. *Clim. Res.* 28, 41–52.
1070 <https://doi.org/10.3354/cr028041>

1071 Plounevez, S., Champalbert, G., 1999. Feeding Behaviour and Trophic Environment
1072 of *Engraulis encrasicolus* (L.) in the Bay of Biscay. *Estuar. Coast. Shelf Sci.* 49, 177–
1073 191. <https://doi.org/10.1006/ecss.1999.0497>

1074 Queiros, Q., Fromentin, J.-M., Gasset, E., Dutto, G., Huiban, C., Metral, L., Leclerc, L.,
1075 Schull, Q., McKenzie, D.J., Saraux, C., 2019. Food in the Sea: Size Also Matters for
1076 Pelagic Fish. *Front. Mar. Sci.* 6.

1077 Romagnan, J.B., Aldamman, L., Gasparini, S., Nival, P., Aubert, A., Jamet, J.L.,
1078 Stemmann, L., 2016. High frequency mesozooplankton monitoring: Can imaging
1079 systems and automated sample analysis help us describe and interpret changes in
1080 zooplankton community composition and size structure - An example from a coastal
1081 site. *J. Mar. Syst.* 162, 18–28. <https://doi.org/10.1016/j.jmarsys.2016.03.013>

1082 Romagnan, J.-B., Legendre, L., Guidi, L., Jamet, J.-L., Jamet, D., Mousseau, L.,
1083 Pedrotti, M.-L., Picheral, M., Gorsky, G., Sardet, C., Stemmann, L., 2015.
1084 Comprehensive Model of Annual Plankton Succession Based on the Whole-Plankton
1085 Time Series Approach. *PLOS ONE* 10, e0119219.
1086 <https://doi.org/10.1371/journal.pone.0119219>

1087 Rykaczewski, R.R., Checkley, D.M., 2008. Influence of ocean winds on the pelagic
1088 ecosystem in upwelling regions. *Proc. Natl. Acad. Sci.* 105, 1965–1970.
1089 <https://doi.org/10.1073/pnas.0711777105>

1090 Saraux, C., Van Beveren, E., Brosset, P., Queiros, Q., Bourdeix, J.-H., Dutto, G.,
1091 Gasset, E., Jac, C., Bonhommeau, S., Fromentin, J.-M., 2019. Small pelagic fish
1092 dynamics: A review of mechanisms in the Gulf of Lions. *Deep Sea Res. Part II Top.*
1093 *Stud. Oceanogr.*, Drivers of dynamics of small pelagic fish resources: environmental
1094 control of long-term changes 159, 52–61. <https://doi.org/10.1016/j.dsr2.2018.02.010>

1095 Saulquin, B., Gohin, F., 2010. Mean seasonal cycle and evolution of the sea surface
1096 temperature from satellite and in situ data in the English Channel for the period 1986–
1097 2006. *Int. J. Remote Sens.* 31, 4069–4093.
1098 <https://doi.org/10.1080/01431160903199155>

1099 Sourisseau, M., Carlotti, F., 2006. Spatial distribution of zooplankton size spectra on
1100 the French continental shelf of the Bay of Biscay during spring 2000 and 2001. J.
1101 Geophys. Res. Oceans 111. <https://doi.org/10.1029/2005JC003063>

1102 Soviadan, Y.D., Benedetti, F., Brandão, M.C., Ayata, S.-D., Irisson, J.-O., Jamet, J.L.,
1103 Kiko, R., Lombard, F., Gnanji, K., Stemmann, L., 2022. Patterns of mesozooplankton
1104 community composition and vertical fluxes in the global ocean. Prog. Oceanogr. 200,
1105 102717. <https://doi.org/10.1016/j.pocean.2021.102717>

1106 Stige, L.C., Dalpadado, P., Orlova, E., Boulay, A.-C., Durant, J.M., Ottersen, G.,
1107 Stenseth, N.Chr., 2014. Spatiotemporal statistical analyses reveal predator-driven
1108 zooplankton fluctuations in the Barents Sea. Prog. Oceanogr. 120, 243–253.
1109 <https://doi.org/10.1016/j.pocean.2013.09.006>

1110 Stirnimann, L., Bornman, T.G., Verheye, H.M., Bachèlery, M.-L., van der Poel, J.,
1111 Fawcett, S.E., 2021. Plankton community composition and productivity near the
1112 Subantarctic Prince Edward Islands archipelago in autumn. Limnol. Oceanogr. 66,
1113 4140–4158. <https://doi.org/10.1002/lno.11949>

1114 Valdes, L., Lopez-Urrutia, A., Beaugrand, G., Harris, R.P., Irigoien, X., 2022.
1115 Seasonality and interannual variability of copepods in the Western English Channel,
1116 Celtic Sea, Bay of Biscay, and Cantabrian Sea with a special emphasis to *Calanus*
1117 *helgolandicus* and *Acartia clausi*. ICES J. Mar. Sci. 79, 727–740.
1118 <https://doi.org/10.1093/icesjms/fsac052>

1119 Van Der Lingen, C.D., 2002. Diet of sardine *Sardinops sagax* in the southern Benguela
1120 upwelling ecosystem. South Afr. J. Mar. Sci. 24, 301–316.
1121 <https://doi.org/10.2989/025776102784528691>

1122 Vandromme, P., Nogueira, E., Huret, M., Lopez-Urrutia, & González-
1123 Nuevo González, G., Sourisseau, M., Petitgas, P., 2014. Springtime zooplankton size
1124 structure over the continental shelf of the Bay of Biscay. Ocean Sci. 10, 821–835.
1125 <https://doi.org/10.5194/os-10-821-2014>

1126 Vandromme, P., Stemmann, L., Garcia-Comas, C., Berline, L., Sun, X., Gorsky, G.,
1127 2012. Assessing biases in computing size spectra of automatically classified
1128 zooplankton from imaging systems: A case study with the ZooScan integrated system.
1129 Methods Oceanogr. 1–2, 3–21. <https://doi.org/10.1016/j.mio.2012.06.001>

1130 Zarauz, L., Irigoien, X., Fernandes, J.A., 2008. Modelling the influence of abiotic and
1131 biotic factors on plankton distribution in the Bay of Biscay, during three consecutive
1132 years (2004-06). *J. Plankton Res.* 30, 857–872. <https://doi.org/10.1093/plankt/fbn049>
1133 Zarauz, L., Irigoien, X., Urtizbera, A., Gonzalez, M., 2007. Mapping plankton
1134 distribution in the Bay of Biscay during three consecutive spring surveys. *Mar. Ecol.*
1135 *Prog. Ser.* 345, 27–39. <https://doi.org/10.3354/meps06970>
1136

1137 **9 Supplementary Materials**

1138 **A. Missing data imputation**

1139 Following the spatial gridding procedure, some data were missing, due to missing
1140 sampling stations in the northern part of the Bay, mostly at the beginning of the time
1141 series (Table A.1). Following Josse & Husson (2016), an algorithm based on iterative
1142 Principal Components Analysis (PCA) from the *MissMDA R* library was used to impute
1143 estimated values in place of the missing ones in the hydrology, phytoplankton and
1144 mesozooplankton datasets. For each variable, the data were organized in matrix grid
1145 cells x years. The first step of the algorithm consisted in the imputation of missing
1146 values with the annual means (for example, if the grid cell numbered 33 had not
1147 Acartiidae's biomass in 2004, it was filled with the 2004 mean Acartiidae's biomass).
1148 Then, a first PCA was performed on the imputed matrix and the estimated values
1149 replaced the annual mean values previously imputed to fill the missing data. Then, a
1150 second PCA was performed and the estimated values from the first PCA were replaced
1151 by the estimated value from the second PCA. The algorithm kept running iteratively
1152 until the difference between two successive estimated values was smaller than a
1153 threshold (set at 1e-06 by default ; Josse & Husson, 2016).

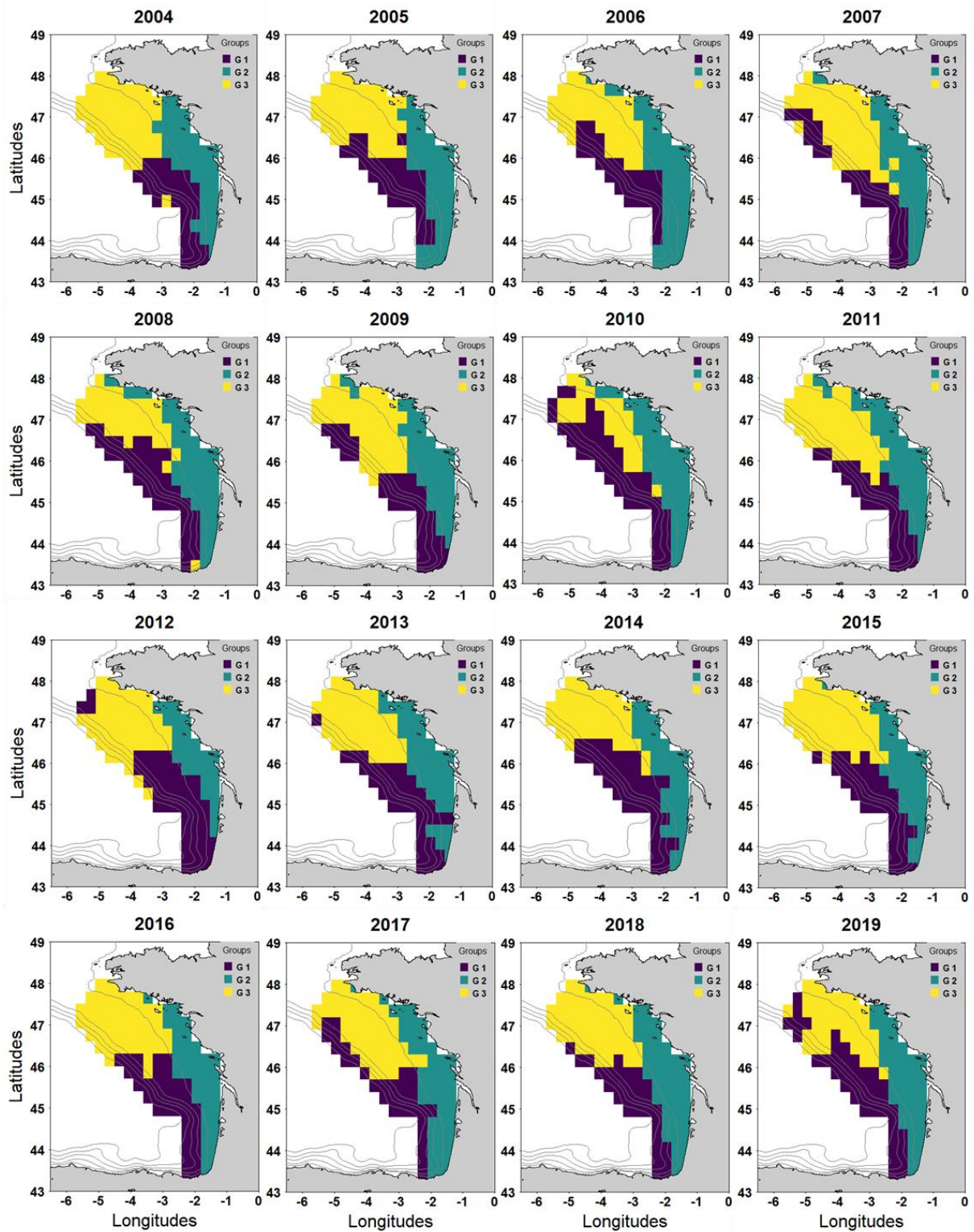
Table A1: Number and percentage of grid cells with missing data each year.

Years	Number of missing cells	Percentage of missing cells
2004	6	5
2005	17	14.1
2006	22	18.2
2007	12	9.9
2008	4	3.3
2009	0	0
2010	0	0
2011	2	1.7
2012	5	4
2013	5	4
2014	2	1.7
2015	0	0
2016	0	0
2017	0	0
2018	0	0
2019	1	0.8

1154

1155

B. Annual spatial clustering



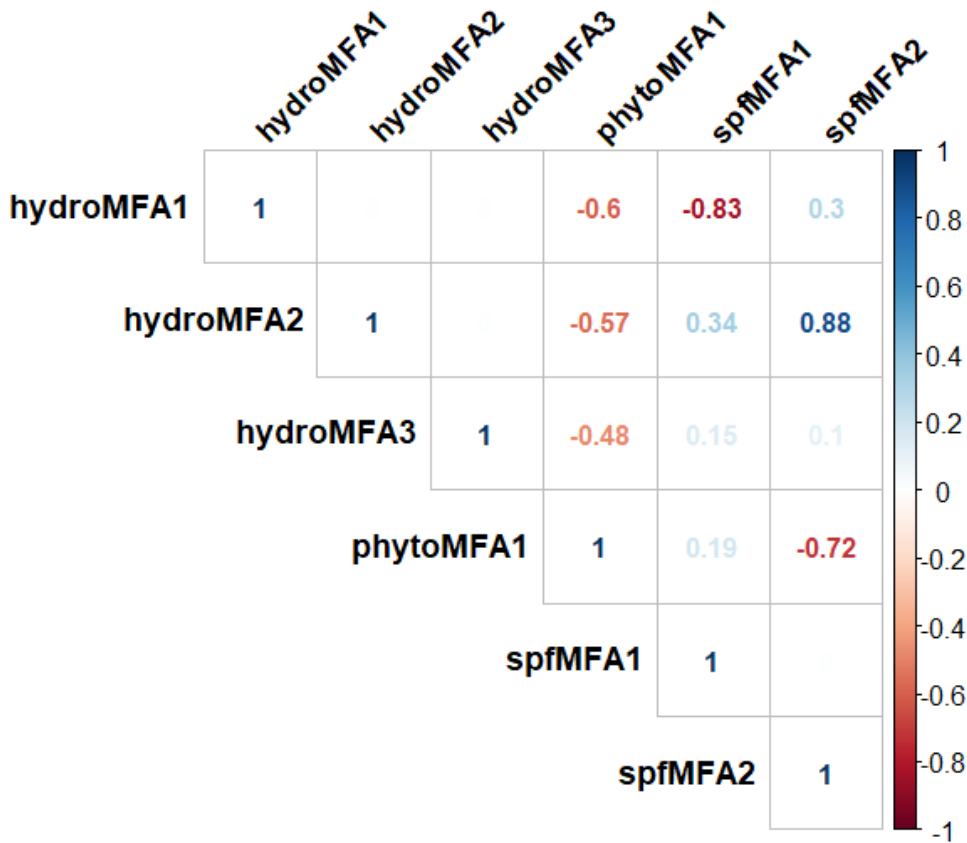
1157 Fig. B1: Annual spatial extent of the clusters identified with the hierarchical clustering of grid
 1158 cells in the mesozooplankton Multi Factor Analysis factorial space.

1160 **C. Correlates of the observed mesozooplankton space-time**
 1161 **patterns**

1162 Table C.1: Variance Inflation Factor (VIF) calculated for each Multi Factor Analysis selected
 1163 principal component in the hydrology, primary producers and small pelagic fish datasets, which
 1164 are used as predictors in Generalized Linear Models. A VIF value higher than five identifies
 1165 problematic multicollinearity among predictors.

Principal components	hydroMFA1	hydroMFA2	hydroMFA3	phytoMFA1	spfMFA1	spfMFA2
VIF values	12.6	13.9	3.7	12.3	7.4	10.1

1166



1167 Fig. C.1: Correlation coefficients among all the predictors.

1168

1169 Table C.2: Results of the stepwise backward model selection procedure showing the models
 1170 explaining the first principal component in the mesozooplankton Multi Factor Analysis
 1171 zooMFA1 and their Akaike's Information Criterion (AIC).

Predictors included in the model	AIC
hydroMFA1 + hydroMFA2 + hydroMFA3 + spfMFA1	450.05
hydroMFA1 + hydroMFA2 + spfMFA1	451.31
hydroMFA1 + hydroMFA3 + spfMFA1	473.49
hydroMFA1 + hydroMFA2 + hydroMFA3	479.17
hydroMFA2 + hydroMFA3 + spfMFA1	491.39

1172

1173 Table C.3 Results of the stepwise backward model selection procedure showing the models
 1174 explaining the second principal component in the mesozooplankton Multi Factor Analysis
 1175 zooMFA2 and their Akaike's Information Criterion (AIC).

Predictors included in the model	AIC
hydroMFA2 + hydroMFA3 + spfMFA1	311.93
hydroMFA2 + spfMFA1	310.57
hydroMFA2	310.73
spfMFA1	771.64

1176

1177